Quantum trajectory approach to circuit QED: Quantum jumps and the Zeno effect

Jay Gambetta,[1,2] Alexandre Blais,[3] M. Boissonneault,[3] A. A. Houck,[1] D. I. Schuster,[1] and S. M. Girvin[1]

[1]*Departments of Applied Physics and Physics, Yale University, New Haven, Connecticut 06520, USA*

[2]*Institute for Quantum Computing and Department of Physics and Astronomy, University of Waterloo, Waterloo, Ontario N2L 3G1, Canada*

[3]*Département de Physique et Regroupement Québécois sur les Matériaux de Pointe, Université de Sherbrooke, Sherbrooke, Québec J1K 2R1, Canada*

We present a theoretical study of a superconducting charge qubit dispersively coupled to a transmission line resonator. Starting from a master equation description of this coupled system and using a polaron transformation, we obtain an exact effective master equation for the qubit. We then use quantum trajectory theory to investigate the measurement of the qubit by continuous homodyne measurement of the resonator out field. Using the same polaron transformation, a stochastic master equation for the conditional state of the qubit is obtained. From this result, various definitions of the measurement time are studied. Furthermore, we find that in the limit of strong homodyne measurement, typical quantum trajectories for the qubit exhibit a crossover from diffusive to jumplike behavior. Finally, in the presence of Rabi drive on the qubit, the qubit dynamics is shown to exhibit quantum Zeno behavior.

PACS number(s): 03.65.Yz, 42.50.Pq, 42.50.Lc, 74.50.+r

I. INTRODUCTION

Continuous-in-time measurement theory [1,2], or quantum trajectory theory, describes how an observer's state of knowledge of a quantum system (known as the conditional state) evolves given a measurement record. Even in the absence of classical noise, such a trajectory follows a stochastic path in time, with the randomness being due to quantum uncertainty. These stochastic trajectories are either diffusive or jumplike in nature. Diffusive trajectories usually arise when the observable being measured is only weakly coupled to the detector [3], whereas jumplike behavior occurs when there is a large sudden change in the observers knowledge of the system state, a typical example of the latter being detection of a photon with a photomultiplier [1,4]. The evolution equation for this trajectory is called a stochastic master equation (SME) [1,2].

In this paper, we consider measurement in circuit quantum electrodynamics (QED) [5–9]. This system consists of a Cooper pair box, playing the role of an artificial atom, dispersively coupled to a one-dimensional (1D) transmission line resonator and is the circuit equivalent of cavity QED. It has the advantage that the qubit can be fixed at an antinode of the resonator which, due to its 1D configuration, has a very large vacuum electric field. This leads to very strong Jaynes-Cummings type coupling between the qubit and the resonator. This allows one to probe a regime of parameter space, where the resonator and qubit are *strongly* coupled via a dispersive interaction and no energy is exchanged between them. In this regime, the qubit causes a large state-dependent shift of the resonator frequency and thus by monitoring the signal transmitted through the resonator we can infer the qubit's state. An important feature of the quasi-one-dimensional circuit resonator is that it permits dispersive couplings $\sim 10^6$ times larger than for ordinary three-dimensional cavities. Coupling of superconducting charge qubits to 3D microwave cavities has also been investigated theoretically [10].

To go beyond previous theoretical works on this system, we employ quantum trajectory theory [1–4,39] and a polaron transformation [11] to derive an effective SME for the qubit. It is well know in quantum optics that if the voltage of a cavity is weakly monitored, then the evolution of the conditional state of the cavity is given by the homodyne SME [1,12]. Using this SME as a starting point, we show that if the rate at which information is coming out of the resonator is much larger then the rate at which information is being lost into unmonitored baths, then we can use a polaron transformation to eliminate the resonator and obtain a SME for the qubit only.

The effective SME which is derived corresponds to a weak dispersive measurement of the qubit observable σ_z. This is akin to SMEs derived in Refs. [13–20] for a quantum dot monitored by a quantum point contact. In Refs. [13–15,18], the SMEs are referred to as the quantum Bayesian equations. They can be seen as the Stratonovich version of the Itô SMEs presented here and in Refs. [17,20]. We note that one can derive a similar equation by adiabatically eliminating the resonator from the qubit-resonator master equation using a similar technique as presented in [21]. However, by using the present method, we are able to derive corrections to the various system rates. These rates are shown to agree very well with the solution of the total resonator-qubit conditional state found by numerically solving the homodyne SME.

The paper is organized as follows. The next section contains a brief discussion of the circuit QED Hamiltonian and of the dispersive approximation. In Sec. III, we use a polaron transformation to eliminate the resonator from the resonator-qubit master equation and in this way obtain an exact master equation for the qubit only. This exact effective master equation shows how the resonator induces an additional dephasing channel on the qubit, whose strength depends on the amplitude of input drives on the resonator. This dephasing rate corresponds to measurement-induced dephasing found in Ref. [9]. It contains the number splitting predicted in Ref. [9,22] and experimentally reported in Ref. [23]. In Sec. IV
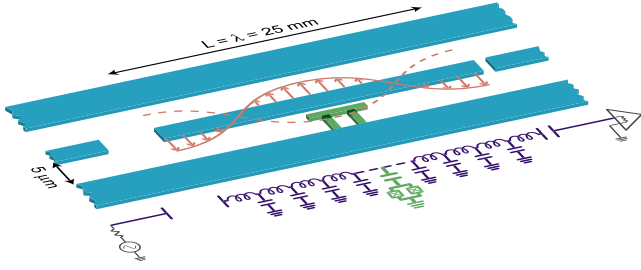
FIG. 1. (Color online) Schematic layout and lumped element version of the circuit QED implementation. A superconducting charge qubit (green) is fabricated inside a superconducting 1D transmission line resonator (blue). Here, we have taken the input [left-hand side (LHS)] and output [right-hand side (RHS)] capacitance of the resonator to be unequal. With the output capacitance much larger than the input one, a larger fraction of the photons in the resonator will escape on the output side. In this way, the signal to be measured is enhanced.

we apply the same polaron transformation to derive an effective SME for the qubit. This equation corresponds to a weak measurement of the qubit σ_z operator with rate Γ_{ci} and extra *non-Heisenberg* backaction which causes random rotations of the qubit around the σ_z with rate Γ_{ba}. Using these results, in Sec. V we investigate the situation where the measurement is quantum limited and how a measurement time can be defined. In Sec. VI, we describe the emergence of quantum jumps in the conditional state as the measurement strength is increased. In particular, we investigate how the spontaneous relaxation into the qubit bath reveals itself as a jump when the measurement is strong, rather than a diffusive decay when the measurement is weak. Finally, in Sec. VII, we include a qubit control drive in our description of the system and investigate how the Zeno effect [24–27] can be observed in this system. We summarize our conclusions in Sec. VIII.

II. CAVITY QED WITH SUPERCONDUCTING CIRCUITS

We consider a Cooper pair box capacitively coupled to a transmission line resonator acting as a simple harmonic oscillator. This system, illustrated schematically in Fig. 1, was first introduced in Ref. [5] and experimentally studied in Refs. [6–8,23,28,29]. Measurement-induced dephasing was theoretically studied in detail in Ref. [9] and the applications to quantum information processing investigated in Ref. [30].

As described in the above references, the system's Hamiltonian in the presence of a microwave drive of amplitude $\varepsilon_d(t)$ and frequency ω_d can be written as [5]

$$H = \frac{\hbar\omega_a}{2}\sigma_z + \hbar\omega_r a^\dagger a + \hbar g(a^\dagger\sigma_- + a\sigma_+)$$
$$+ \hbar[\varepsilon_d(t)a^\dagger e^{-i\omega_d t} + \varepsilon_d^*(t)a e^{i\omega_d t}]. \tag{2.1}$$

In this expression, ω_r is the resonator frequency, ω_a the qubit transition frequency, and g the resonator-qubit coupling strength. Depending on its frequency, the drive can correspond either to measurement of the qubit or can be used to

coherently control its state. In the dispersive regime, when $|\Delta| = |\omega_a - \omega_r| \gg |g|$, the effective Hamiltonian, Eq. (2.1), can be approximated by [5]

$$H_{\text{eff}} = \frac{\hbar\widetilde{\omega}_a}{2}\sigma_z + \hbar\Delta_r a^\dagger a + \hbar\chi a^\dagger a\sigma_z + \hbar[\varepsilon_d(t)a^\dagger + \varepsilon_d^*(t)a],$$
$$\tag{2.2}$$

where $\Delta_r = \omega_r - \omega_d$ and we have assumed that the drive is far off resonance from the qubit transition frequency and moved the resonator to a frame rotating at frequency ω_d. In this expression, we have defined $\chi = g^2/\Delta$ as the dispersive coupling strength between the resonator photon number and the qubit. Moreover, we have taken $\widetilde{\omega}_a = \omega_a + \chi$ as the Lamb shifted qubit transition frequency and defined $\Delta_r = \omega_r - \omega_d$.

It is important to note that the dispersive approximation breaks down as the number of photons in the resonator approaches the critical photon number $n_{\text{crit}} = \Delta^2/4g^2$ [5]. In the present paper, we will work at moderately low photon number and assume the dispersive approximation to hold. That is, we will assume that Eq. (2.2) is a valid description of the system. The results obtained will therefore also apply to the circuit QED implementation that uses the so-called transmon qubit [31]. A future publication will explore the break down of the dispersive approximation [32] at small detuning and large photon number.

III. MASTER EQUATION

A. Master equation for the combined system

In the Born-Markov approximation, the master equation describing circuit QED takes the usual Lindblad form [1,33]

$$\dot{\varrho}(t) = -\frac{i}{\hbar}[H_{\text{eff}}, \varrho(t)] + \kappa\mathcal{D}[a]\varrho(t) + \gamma_1\mathcal{D}[\sigma]\varrho(t)$$
$$+ \gamma_\phi\mathcal{D}[\sigma_z]\varrho(t)/2 = \mathcal{L}_{\text{tot}}\varrho(t), \tag{3.1}$$

where $\varrho(t)$ is the state matrix for both the qubit and the resonator and $\mathcal{D}[A]$ is the damping superoperator defined by the mapping

$$\mathcal{D}[A]\varrho = A\varrho A^\dagger - A^\dagger A\varrho/2 - \varrho A^\dagger A/2. \tag{3.2}$$

The three damping channels are photon loss through the resonator (κ), qubit decay (γ_1), and dephasing of the qubit (γ_ϕ) [34].

There are two distinct contributions to the resonator damping: loss of photon from the input port described by the rate κ_{in} and loss of photons at the output port κ_{out}. The sum of these two rates $\kappa = \kappa_{\text{in}} + \kappa_{\text{out}}$ is what appears in Eq. (3.1). The advantage of distinguishing these two contributions is that, in current experiments, only the photons leaking out of the output port are monitored. Hence, as we will see later, κ_{out} is related to the rate at which we acquire information about the qubit state.

B. Master equation for the qubit

In Ref. [9] the solution of the above master equation, neglecting energy loss due to γ_1 (but keeping its effect on dephasing), was found to be

$$\varrho(t) = \sum_{i,j=e,g} c_{i,j}(t)|i\rangle\langle j| \otimes |\alpha_i(t)\rangle\langle\alpha_j(t)|, \qquad (3.3)$$

where the indices g and e label the qubit ground and excited states, respectively. In this expression, the coefficients $c_{i,j}(t)$ are given by

$$c_{e,e}(t) = c_{e,e}(0), \quad c_{g,g}(t) = c_{g,g}(0),$$

$$c_{e,g}(t) = \frac{c_{e,g}(0)e^{-i(\tilde{\omega}_a - i\gamma_2)t}e^{-i2\chi\int_0^t \alpha_e(s)\alpha_g^*(s)ds}}{\langle\alpha_g(t)|\alpha_e(t)\rangle},$$

$$c_{g,e}(t) = c_{e,g}^*(t), \qquad (3.4)$$

and $|\alpha_{e(g)}(t)\rangle$ are coherent states of the resonator with amplitudes determined by

$$\dot{\alpha}_e(t) = -i\varepsilon_d(t) - i(\Delta_r + \chi)\alpha_e(t) - \kappa\alpha_e(t)/2,$$

$$\dot{\alpha}_g(t) = -i\varepsilon_d(t) - i(\Delta_r - \chi)\alpha_g(t) - \kappa\alpha_g(t)/2. \qquad (3.5)$$

In the expression for $c_{e,g}(t)$, we see that in addition to decay due to dephasing $\gamma_2 = \gamma_1/2 + \gamma_\phi$, the off-diagonal element of the qubit density matrix decays at a rate that depends on the field amplitudes α_g and α_e. Since the coherent states with these amplitudes act as pointer states in the measurement of the qubit, this decay can be interpreted as measurement-induced dephasing and will depend on how distinguishable the states $|\alpha_e(t)\rangle$ and $|\alpha_g(t)\rangle$ are [9]. Following Ref. [9], the effect of qubit relaxation in this model has been described by Bonzom *et al.* [35].

How these coherent states act as pointer states for the qubit is illustrated in Fig. 2, where a phase-space representation of the resonator state $\mathrm{Tr}_{\mathrm{qubit}}[\varrho(t)]$ is plotted for various qubit-field interaction times. In these plots, the initial state is taken to be the vacuum for the resonator and the symmetric superposition $(|e\rangle+|g\rangle)/\sqrt{2}$ for the qubit. A continuous coherent drive is turned on at time $t=50$ ns to build up photon population of the resonator. The three panels of Fig. 2 illustrate how the two coherent states $|\alpha_e(t)\rangle$ and $|\alpha_g(t)\rangle$ eventually become separated in phase space. Homodyne detection of the resonator field, with the proper choice of local oscillator phase ϕ, can then be used to distinguish between these two coherent states and thus readout the state of the qubit. In the last panel of Fig. 2 we have introduced the distance between the states $|\alpha_e(t)\rangle$ and $|\alpha_g(t)\rangle$,

$$\beta(t) = \alpha_e(t) - \alpha_g(t). \qquad (3.6)$$

Another useful quantity is the angle

$$\theta_\beta = \arg(\beta). \qquad (3.7)$$

For example, for the case of Fig. 2(c), this angle is $\theta_\beta = \pi$, which corresponds to the quadrature containing the most information about the state of the qubit. Indeed, for this particular case, all of the information is in the in-phase component I, with no information stored in the quadrature Q component.

Our goal in the remainder of this section is to obtain an effective master equation for the qubit by eliminating the
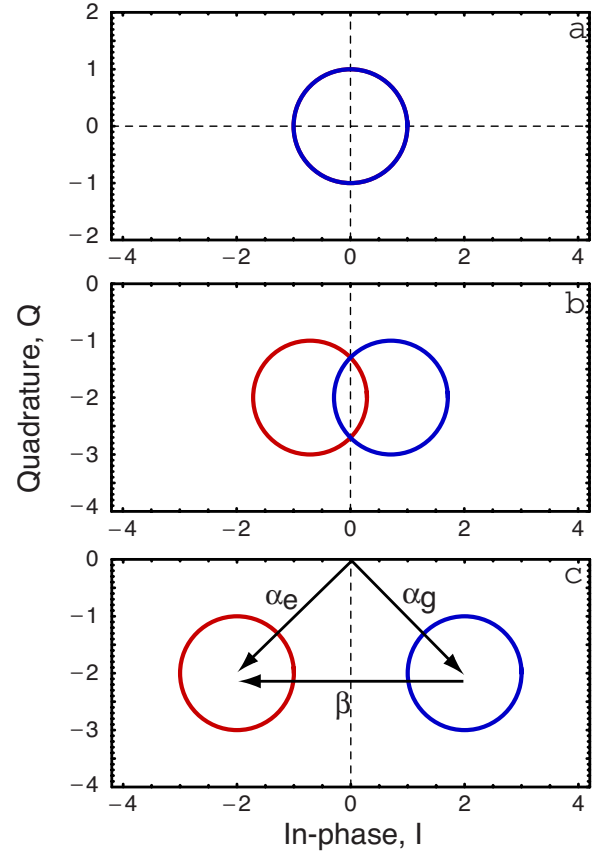

FIG. 2. (Color online) In-phase $I = \mathrm{Re}[\langle a\rangle] = \langle a+a^\dagger\rangle/2$ and quadrature $Q = \mathrm{Im}[\langle a\rangle] = \langle ia^\dagger - ia\rangle/2$ component of the Q-function solution for the resonator state $\mathrm{Tr}_{\mathrm{qubit}}[\varrho_s]$. Here the parameters are $\kappa/2\pi = 10$ MHz, $\chi/2\pi = 5$ MHz, $\epsilon/2\pi = 20$ MHz, and $\Delta_r = 0$. The measurement drive is turned on at $t=50$ ns and the initial state is $|0\rangle \otimes (|e\rangle + |g\rangle)/\sqrt{2}$. For illustration purposes, γ_1 was taken to be zero. (a) $t=0$, (b) $t=75$ ns, (c) Steady-state solution.

resonator degree of freedom from the full master equation, Eq. (3.1). To achieve this, we first go to a frame defined by the transformation

$$\mathbf{P}(t) = \Pi_e D[\alpha_e(t)] + \Pi_g D[\alpha_g(t)] \qquad (3.8)$$

with $D[\alpha]$ the displacement operator of the resonator,

$$D[\alpha] = \exp[\alpha a^\dagger - \alpha^* a], \qquad (3.9)$$

and $\Pi_j = |j\rangle\langle j|$ projectors on the ground and excited states of the qubit. This is similar to the polaron transformation which has been used extensively in various systems [11,36]. For example, this was used in Ref. [37] to study a charge qubit coupled to a mechanical oscillator beyond the rotating wave approximation. However, here we use the transformation, Eq. (3.8), on the dispersive Hamiltonian, not on the full Jaynes-Cummings Hamiltonian.

As is shown in Appendix A, applying this transformation on the master, Eq. (3.1), and tracing over the resonator state yields the laboratory frame reduced qubit master equation

$$\dot{\rho}(t) = -i\frac{\omega_{\mathrm{ac}}(t)}{2}[\sigma_z, \rho(t)] + \gamma_1 \mathcal{D}[\sigma_-]\rho(t)$$

$$+ [\gamma_\phi + \Gamma_{\mathrm{d}}(t)]\mathcal{D}[\sigma_z]\rho(t)/2 = \mathcal{L}\rho(t), \qquad (3.10)$$

where $\rho(t) = \mathrm{Tr}_{\mathrm{res}}[\varrho(t)]$. This expression is the main result of this section. It is important to note that, within the dispersive approximation, this result is exact.

In this reduced description, we see that the effect of coupling to the resonator translates into an additional dephasing rate $\Gamma_{\mathrm{d}}(t)$ given by

$$\Gamma_{\mathrm{d}}(t) = 2\chi \, \mathrm{Im}[\alpha_g(t)\alpha_e^*(t)]. \qquad (3.11)$$

In addition to dephasing, the qubit transition frequency is also modified by the photon population of the resonator. The shifted qubit frequency is given by

$$\omega_{\mathrm{ac}}(t) = \tilde{\omega}_a + B(t) \qquad (3.12)$$

with

$$B(t) = 2\chi \, \mathrm{Re}[\alpha_g(t)\alpha_e^*(t)]. \qquad (3.13)$$

This last term gives rise to the ac-stark shift experimentally measured in Ref. [8]. In the situation where $\chi \gg \kappa$, the above leads to the number splitting predicted in Ref. [9,22] and experimentally observed in Ref. [23].

Although the above results are analytically exact, we have compared the numerical solution of the qubit's dynamics obtained from the full master equation, Eq. (3.1), to that obtained from the reduced model equation, Eq. (3.10). This is shown in Fig. 3 where the elements of the Bloch vector are plotted as a function of time. It is useful to note that, in terms of the Bloch vector,

$$\rho(t) = \frac{1}{2}[1 + x(t)\sigma_x + y(t)\sigma_y + z(t)\sigma_z], \qquad (3.14)$$

where $x(t) = \mathrm{Tr}[\sigma_x \rho(t)]$, $y(t) = \mathrm{Tr}[\sigma_y \rho(t)]$, and $z(t) = \mathrm{Tr}[\sigma_z \rho(t)]$, the effective master equation, Eq. (3.10), reduces to the simple Bloch equations

$$\dot{x}(t) = -\omega_{\mathrm{ac}}(t)y(t) - [\gamma_2 + \Gamma_{\mathrm{d}}(t)]x(t),$$

$$\dot{y}(t) = \omega_{\mathrm{ac}}(t)x(t) - [\gamma_2 + \Gamma_{\mathrm{d}}(t)]y(t),$$

$$\dot{z}(t) = -\gamma_1[z(t) + 1]. \qquad (3.15)$$

Not surprisingly, as seen from Fig. 3, the agreement between numerical integration of these Bloch equations and full numerical integration of the full master equation is excellent. The agreement between these two results can be quantified by calculating the trace distance $d_{\mathrm{Tr}}(t)$ between the full and the effective model. The trace distance in this case is defined as [38]

$$d_{\mathrm{Tr}}(t) = \frac{1}{2} \, \mathrm{Tr}\{|\rho(t) - \mathrm{Tr}_{\mathrm{res}}[\varrho(t)]|\}, \qquad (3.16)$$

and is found to be zero at all integration times, up to numerical round off (truncation) errors. This was checked for a wide range of measurement amplitudes ε_d and the trace distance was also found to be zero for all verified amplitudes. Also in
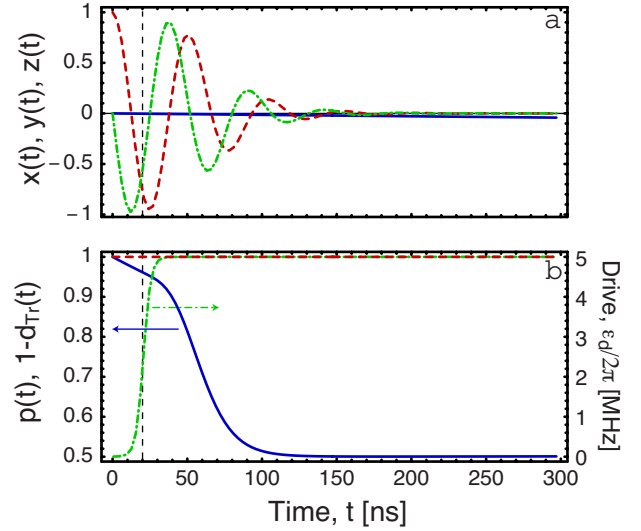

FIG. 3. (Color online) (a) Numerical solution of the three components of the Bloch vector as obtained from the full master equation: x (red dashed line), y (green dashed-dotted line), and z (solid blue line). For this simulation, a measurement drive tuned at the resonator frequency ($\Delta_r = 0$) and with envelope $\varepsilon_{\mathrm{d}}(t) = A \tanh[(t - t_{\mathrm{on}})/\sigma]$ is turned on at $t_{\mathrm{on}} = 20$ ns [green dashed-dotted line in panel (b)]. The turn-on time is indicated with the vertical dashed line. (b) Purity p (solid blue line) and the trace distance d_{Tr} (red dashed line) with respect to the effective model derived here. The latter shows the excellent agreement between the model and full numerical results. For these results, we have taken $A/2\pi = 5$ MHz, $\sigma = 5$ ns, $T_1 = 7$ μs, and $T_2 = 500$ ns. The other parameters are the same as in Fig. 2.

this figure is shown the purity (full blue line)

$$p(t) = \mathrm{Tr}[\rho(t)^2] = \frac{1}{2}[1 + x(t)^2 + y(t)^2 + z(t)^2]. \qquad (3.17)$$

In this master equation description, the purity tends to 1/2, corresponding to a completely mixed state, due to dephasing. On top of this dynamics, relaxation is taking the purity to 1 (a pure state) at a rate γ_1. For the parameters chosen in Fig. 3 relaxation is much weaker than (measurement-induced) dephasing, such that only the effect of the latter is seen.

To summarize this section, we have obtained an *exact* master equation description of the qubit dynamics that only involves classical solution of the resonator field. In addition to giving direct insights in the qubits dynamics (e.g., measurement-induced dephasing and ac-Stark shift) this also provides a tool to significantly reduce the complexity of numerical calculations. Indeed, only a two-dimensional Hilbert space is now required. We note that this effective model was used to analyze and reproduce, with exceptional agreement, the experimental results reported in Ref. [28].

IV. STOCHASTIC MASTER EQUATION

A. Stochastic master equation for the combined system

In this section, we review homodyne measurement of the field emitted from the resonator. Using these results, we will

in Sec. IV B use the transformation of Eq. (3.8) to obtain an effective SME for the qubit only.

In a given quantum system, if all the decoherence and decay channels can be monitored continuously, it is possible to describe the system conditioned on the results of this monitoring result $J(t)$ by a pure state $|\Psi_J\rangle$ rather than by the average state ϱ. This pure states is called a conditional state and can be viewed as our state of knowledge of the system. However, in systems where information about only some of the decay channels can be obtained, there is missing information, and it is no longer possible to have a pure state description. In this case, we can assign a conditional state matrix, ϱ_J, to represent the state of the system under continuous observation of the particular decay channels. The evolution equation of this conditional state is referred to as a stochastic master equation (SME) [1–4,12,14,18,39]. It has the property that its average state $\varrho(t)$,

$$\varrho(t) = E[\varrho_J(t)], \qquad (4.1)$$

is the solution to the master equation. Here E denotes an ensemble average over measurement records $J(t)$.

In circuit QED, there are four decay channels described by the rates κ_{in}, κ_{out}, γ_1, and γ_ϕ. Only information coming out of the κ_{out} channel, that is photons transmitted through the resonator, are monitored. As a result, we must restrict our description to a conditional density matrix. As will be discussed in the next section, in the effective model for the qubit only, this will correspond to monitoring the decay channel corresponding to the rate $\Gamma_d(t)$ and not monitoring the γ_1 and γ_ϕ channels.

Although direct detection of the transmitted microwave photons is possible [28], here we will consider homodyne processing. That is, we will assume that the signal coming from the output port of the resonator is mixed with a strong local oscillator of phase ϕ tuned to the signal frequency. Given the homodyne measurement result $J(t)$, we can assign to the qubit-resonator system the conditional state $\varrho_J(t)$ whose evolution is governed by the SME [40]

$$\dot{\varrho}_J(t) = \mathcal{L}_{tot}\varrho_J(t) + i\sqrt{\kappa\eta}[Q_\phi, \varrho_J][J(t) - \sqrt{\kappa\eta}\langle 2I_\phi\rangle_t]$$
$$+ \sqrt{\kappa\eta}\mathcal{M}[2I_\phi]\varrho_J(t)[J(t) - \sqrt{\kappa\eta}\langle 2I_\phi\rangle_t] \qquad (4.2)$$

with $\mathcal{L}_{tot}$ given by Eq. (3.1), η is the measurement efficiency which we define below, $\mathcal{M}[c]$ is the measurement superoperator defined as

$$\mathcal{M}[c]\varrho = (c - \langle c\rangle_t)\varrho/2 + \varrho(c - \langle c\rangle_t)/2, \qquad (4.3)$$

where $\langle c\rangle_t = \mathrm{Tr}[c\varrho_J(t)]$ and the ϕ-dependent field components are $2I_\phi = ae^{-i\phi} + a^\dagger e^{i\phi}$ and $2Q_\phi = -iae^{-i\phi} + ia^\dagger e^{i\phi}$. The efficiency is $\eta = \kappa_{out}\eta_{det}/\kappa$ with κ_{out} the rate at which photons come out of the output port of the resonator and η_{det} is the efficiency at which these photons are detected. For the current circuit QED experiments [6–8,23,28,29], this can be written as $\eta_{det} = 1/(N+1)$ with N the number of noise photons added by the amplifier stage.

For homodyne detection, the measurement record observed in an experiment can be expressed as

$$J(t) = \sqrt{\kappa\eta}\langle 2I_\phi\rangle_t + \xi(t), \qquad (4.4)$$

where $\xi(t)$ is Gaussian white noise and represents the photon shot noise. It is formally defined as [41]

$$E[\xi(t)] = 0, \qquad (4.5)$$

$$E[\xi(t)\xi(t')] = \delta(t - t'), \qquad (4.6)$$

with E denoting an ensemble average over realizations of the noise $\xi(t)$.

The measurement term in Eq. (4.2), the one including the superoperator $\mathcal{M}[2I_\phi]$, comprises two parts. We will refer to the first one as the homodyne gain and the second as the innovation. The homodyne gain is $\sqrt{\kappa\eta}\mathcal{M}[2I_\phi]\varrho_J(t)$ and collapses the state towards a I_ϕ state (eigenstate of I_ϕ). The innovation is $J - \sqrt{\kappa\eta}\langle 2I_\phi\rangle_t$, it pushes the conditional state to a higher or lower I_ϕ state depending on whether the current result $J(t)$ is greater or smaller then the average $\sqrt{\kappa\eta}\langle 2I_\phi\rangle_t$. The last term in Eq. (4.2), the noisy Hamiltonian term is extra non-Heisenberg backaction (it does not come with any information gain) caused by the measurement. It is this term that stops the conditional state from being driven to a I_ϕ state as it supplies random Q_ϕ kicks to the conditional state causing delocalization in I_ϕ.

For heterodyne measurement [where the local oscillator (LO) is detuned from the signal frequency], both component I_ϕ and Q_ϕ can be measured simultaneously. In this case, the SME, Eq. (4.2), has extra gain and innovation terms corresponding to this additional component. Heterodyne measurement also lowers the measurement efficiency η_{det} by a factor of $1/2$. Detection of this second component does not change the physics in an essential way, and we will focus on the simpler case of homodyne detection in the remainder of this paper.

Finally, we note that the SME, Eq. (4.2), is known to lead to a diffusivelike evolution for the system [3,12,42]. We will however see in Sec. VI how there can be a crossover from diffusive to jumplike evolution as the measurement strength is increased.

B. Stochastic master equation for the qubit

In this section, we use the transformation Eq. (3.8) to obtain an effective SME for the qubit only. As described in Appendix B, this can be done in the limit where

$$\epsilon = \frac{2\gamma_1}{\kappa} \ll 1. \qquad (4.7)$$

We note that this limit does not imply that the information gain about the state of the qubit is small. For the system to be in this limit, we simply require that the photons come out of the resonator faster than the qubit decay rate. Otherwise, the full SME of Eq. (4.2) must be used. However, as will be seen from numerical investigations, the validity of the model can extend well beyond this limit in practice.

As described in Appendix B, in the limit where Eq. (4.7) is valid, the effective SME for the qubit obtained using the transformation of Eq. (3.8) and tracing over the resonator states is

$$\dot{\rho}_{\bar{J}}(t) = \mathcal{L}\rho_{\bar{J}}(t) + \sqrt{\Gamma_{ci}(t)}\mathcal{M}[\sigma_z]\langle\sigma_z\rangle\rho_{\bar{J}}(t)[\bar{J}(t) - \sqrt{\Gamma_{ci}(t)}\langle\sigma_z\rangle_t]$$

$$- i\frac{\sqrt{\Gamma_{ba}(t)}}{2}[\sigma_z, \rho_{\bar{J}}(t)][\bar{J}(t) - \sqrt{\Gamma_{ci}(t)}\langle\sigma_z\rangle_t]. \quad (4.8)$$

In this expression, $\Gamma_{ci}(t)$ is the rate at which coherent information comes out the resonator and $\Gamma_{ba}(t)$ represents extra non-Heisenberg backaction from the measurement. These rates are given by

$$\Gamma_{ci}(t) = \eta\kappa|\beta(t)|^2 \cos^2(\phi - \theta_\beta), \quad (4.9)$$

$$\Gamma_{ba}(t) = \eta\kappa|\beta(t)|^2 \sin^2(\phi - \theta_\beta), \quad (4.10)$$

with the angle θ_β being defined in Eq. (3.7).

In Eq. (4.8), $\bar{J}(t)$ is the processed record coming from the resonator and is given by

$$\bar{J}(t) = \sqrt{\Gamma_{ci}}\langle\sigma_z\rangle_t + \xi(t), \quad (4.11)$$

which can be related to the homodyne current by

$$J(t) = \bar{J}(t) + \sqrt{\kappa\eta}|\mu(t)|\cos(\theta_\mu - \phi) \quad (4.12)$$

with $\mu(t) = \alpha_e(t) + \alpha_g(t)$ and $\theta_\mu = \arg(\mu)$.

From the above expressions, by doing homodyne measurement on the field leaving the resonator we are in fact doing a weak diffusive measurement of the qubit operator σ_z with measurement strength $\Gamma_{ci}(t)$, as well as causing extra unitary backaction on the qubit [by the term proportional to $\Gamma_{ba}(t)$]. This is clearly seen by rewriting Eq. (4.8) in terms of the Bloch vectors

$$\dot{x}_J(t) = -\{\omega_{ac}(t) + \sqrt{\Gamma_{ba}(t)}[\bar{J}(t) - \sqrt{\Gamma_{ci}(t)}z_J(t)]\}y_J(t)$$

$$- \{\gamma_2 + \Gamma_d(t) + \sqrt{\Gamma_{ci}(t)}z_J(t)[\bar{J} - \sqrt{\Gamma_{ci}(t)}z_J]\}x_J(t),$$

$$\dot{y}_J(t) = \{\omega_{ac}(t) + \sqrt{\Gamma_{ba}(t)}[\bar{J}(t) - \sqrt{\Gamma_{ci}(t)}z_J(t)]\}x_J(t)$$

$$- \{\gamma_2 + \Gamma_d(t) + \sqrt{\Gamma_{ci}(t)}z_J(t)[\bar{J} - \sqrt{\Gamma_{ci}(t)}z_J]\}y_J(t),$$

$$\dot{z}_J(t) = \sqrt{\Gamma_{ci}(t)}[1 - z_J(t)^2][\bar{J}(t) - \sqrt{\Gamma_{ci}(t)}z_J(t)] - \gamma_1[z_J(t) + 1].$$

$$(4.13)$$

From these expression, we see that the effect of the measurement consists of two parts. First, a nonlinear update to the state which results in pushing the system towards either $z = \pm 1$ depending on the observed record [the terms proportional to $\Gamma_{ci}(t)$], and second, an extra stochastic component that causes rotations around the σ_z axis [the $\Gamma_{ba}(t)$ terms]. We find that the sum of these rates is $\eta\Gamma_m(t)$ where

$$\Gamma_m(t) = \kappa|\beta(t)|^2 \quad (4.14)$$

is the maximum measurement rate. This rate can be simply understood by noting that κ is the rate at which photons leak out the resonator and $|\beta(t)|^2$ is the amount of information about the qubit state encoded by these photons. That is, this is the maximum amount of information that can be gained from this system via homodyne monitoring. Looking at Eq. (4.9) this is achieved by setting the homodyne phase to θ_β
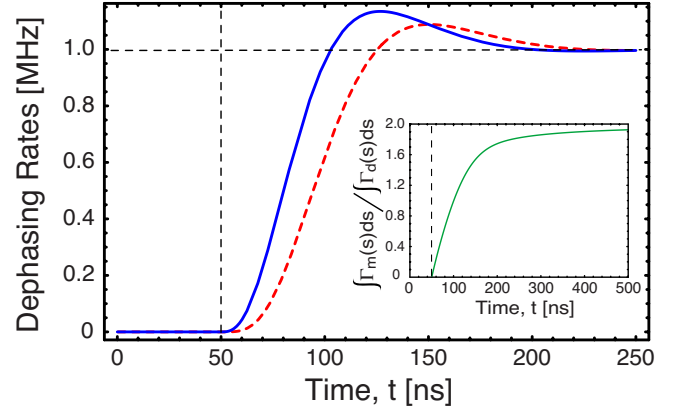

FIG. 4. (Color online) $\Gamma_d(t)$ (solid blue line) and $\Gamma_m(t)/2$ (dashed red line) for a measurement drive turned on at the time $t = 50$ ns. The drive frequency is tuned to the bare resonator frequency ($\Delta_r = 0$) and the amplitude is $\varepsilon_m/2\pi = \sqrt{5}$. The rest of the parameters are the same as in Fig. 2. The inset shows the ratio between the total dephasing and the total measurement-induced dephasing. The vertical black dashed line is the turn on time for the measurement drive. The horizontal dashed line is the steady-state dephasing rate.

and physically corresponds to detecting the quadrature which has the greatest separation of the pointer states [see Fig. 2(c)]. If we set ϕ to be $\theta_\beta + \pi/2$, then $\Gamma_{ba}(t) = \eta\Gamma_m(t)$, which results in the measurement revealing no information about the qubit state and only causing dephasing by qubit frequency change via photon shot noise.

When the resonator dynamics have reached steady state, it can be shown that

$$\Gamma_d(t \to \infty) = \Gamma_m(t \to \infty)/2. \quad (4.15)$$

This is illustrated in Fig. 4 where both $\Gamma_d(t)$ (solid blue line) and $\Gamma_m(t)/2$ (dashed red line) are presented for the situation where a measurement drive tuned to the bare resonator frequency is turned on at $t = 50$ ns. From this figure, we see that after the resonator transients decay away, the dephasing rate Γ_d is twice the maximum measurement rate Γ_m. Also shown in the figure (see inset) is the ratio between the total dephasing of the system, which we define as $\int_0^t \Gamma_d(s)ds$, and the total measurement-induced dephasing, defined as $\int_0^t \Gamma_m(s)ds/2$. As it should (when $\kappa \gg \chi$), the former exceeds, or is at least equal to, the latter. This is simply a statement that there is additional information about the qubit available in the initial transients of the resonator which is not being used when simply monitoring the homodyne signal.

A typical trajectory for the conditional state is shown in Fig. 5(a) (red dashed line is the x component, green dashed-dotted line is the y component, and the solid blue line is the z component) for the case of a measurement drive turned on at $t_{on} = 20$ ns and of maximal amplitude $\varepsilon_d^{max}/2\pi = 5$ MHz. The envelope of the drive, shown as the green dashed-dotted line in Fig. 5(b), is the same shape as the one used in Fig. 3.

Unlike the average evolution, as we monitor the system we become more certain of its quantum state. This is represented in Fig. 5(a) by the z component being stochastically
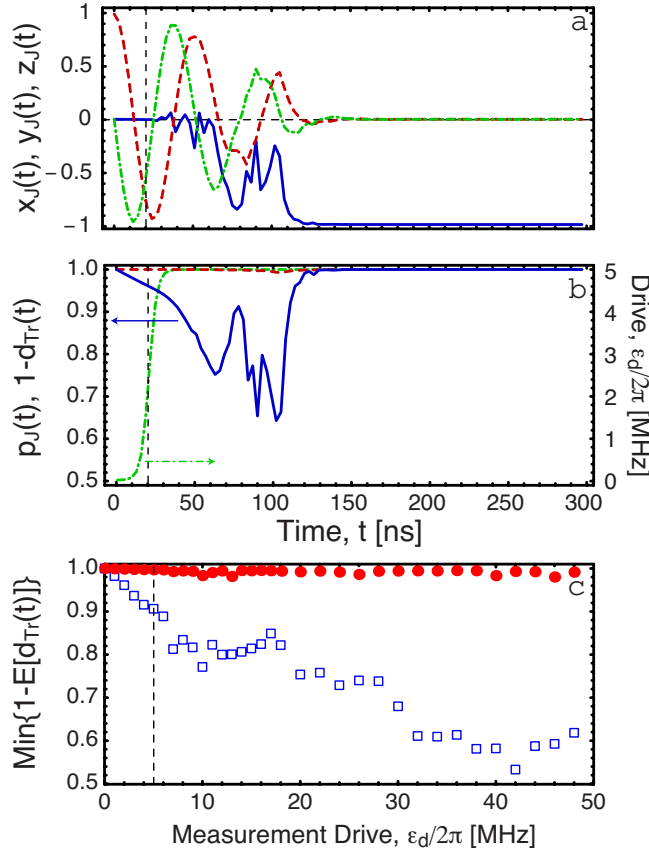
FIG. 5. (Color online) (a) Numerical solution of the three components of the Block vector as obtained from the full homodyne SME: x, red dashed line; y, green dashed-dotted line; z, solid blue line. The measurement frequency and envelope is the same as in Fig. 3. We have assumed perfect efficiency $\eta=1$ and taken the LO phase to be $\phi=\theta_\beta=\pi$, corresponding to maximal information gain at $\Delta_r=0$. (b) Conditional purity p_J (full blue line) and measurement pulse amplitude (dotted-dashed green line). Also shown is one minus the trace distance (dashed red line), as calculated from the full homodyne SME and the effective SME. (c) One minus the trace distance minimized over the simulation time, 300 ns, for a range of measurement amplitude and two values of T_1: 7 μs (full red dots), 100 ns (empty blue squares). Here, the trace distance is averaged over 70 trajectories.

pushed towards $z=-1$. Note that we are showing but one possible trajectory, other realizations will tend to localize the z component to $+1$. The fact that our state of knowledge about the quantum state is increased by monitoring is also made apparent by the purity which reaches unity [full blue line in Fig. 5(b)]. Under the average evolution, see Fig. 3(b), we end up with a completely mixed state. This is simply due to the fact that the average description does not take into account the information gain due to the measurement.

Also shown in Fig. 5(b) is the trace distance between the conditional state found using the homodyne SME, Eq. (4.2) and the effective SME, Eq. (4.8), in both cases using the same parameters as in Fig. 5(a). The agreement between the two results is excellent, which shows that when the limit, Eq. (4.7), is valid, the effective model derived here is indeed a good description. To see the breakdown of the validity of the

model, we plot in Fig. 5(c) one minus the trace distance minimized over the simulation time, 300 ns, as a function of measurement amplitude and for two values of T_1. This is calculated and averaged over 70 trajectories. For $T_1=7$ μs (full red circles), the agreement is very good at all simulated amplitudes. However, for $T_1=100$ ns (empty blue squares), the condition, Eq. (4.7), is much less valid. As the measurement amplitude is increased, the approximation that we can neglect elements of Eqs. (B10) and (B11) in Eq. (B9) breaks down and the discrepancy between the effective and full models is apparent. In any cases, it is clear that the effective model is a *very* good approximation for long T_1 and can give a relatively accurate description of the system even at low T_1, provided that the measurement amplitude is not too large. We note that a T_1 of 7 μs was reported in Ref. [7]. The model obtained here is therefore useful in realistic experimental settings.

Moreover, we find that for the small T_1 of 100 ns, while the discrepancy reported in Fig. 5(c) for an average over many trajectories can be large, when inspecting single trajectories we find no notable new features as the measurement amplitude is increased. The only change can be attributed to renormalization of the various systems parameters under the measurement. This suggests that the effective model presented here may extend well beyond the limit (4.7), with the only change being that the measurement rate must be obtained numerically (or experimentally measured).

C. Signal-to-noise ratio

Using the above results, we can define the signal-to-noise ratio (SNR) as

$$\text{SNR} = \frac{\Gamma_{\text{ci}}}{\gamma_1} = \frac{\eta \Gamma_{\text{m}} \cos^2(\theta_\beta - \phi)}{\gamma_1}. \quad (4.16)$$

As expected, the SNR is maximized by setting the phase ϕ of the local oscillator to the quadrature containing the most information: $\phi=\theta_\beta$ (see Fig. 2). Since Γ_{m} scales with the measurement amplitude, and thus with the number of photons populating the resonator, this expression indicates that arbitrarily large SNRs can be reached in principle by simply increasing this amplitude. However, as was also pointed out in Ref. [5], at large photon numbers the dispersive Hamiltonian, Eq. (2.2), breaks down and the results obtained here are simply no longer valid.

As a result, we must maximize the SNR at a fixed number of photons which is assumed to be small enough for the dispersive approximation to be valid. The number of photons inside the resonator depends on the drive amplitude ε_d, on resonator damping κ, resonator-drive detuning Δ_r, and on the dispersive qubit-resonator coupling χ. Because of the latter, the actual number of photons can depend on the state of the qubit. We thus define n_g and n_e the number of photons given that the qubit is in the ground or excited state [9]. When optimizing, we therefore work at a fixed $n=\max(n_e,n_g)$, which is assumed to be well below the dispersive breakdown. Under this constraint, and assuming that the resonator has reached steady state, we find that the optimal SNR, for arbitrary χ and κ, occurs at $\Delta_r=0$ and is given by
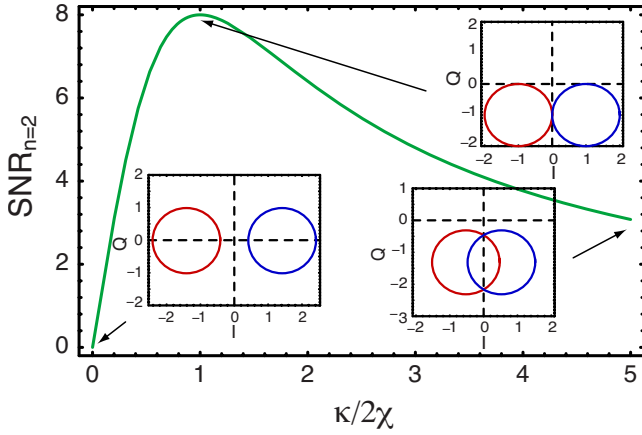
FIG. 6. (Color online) The signal-to-noise ratio (SNR) at $\Delta_r =0$ and for a fixed number of photons in the resonator $n=2$. The efficiency was taken to be ideal $\eta=1$ and the relation rate $\gamma_1/2\pi =1$ MHz. The three insets show the phase space representation of the resonator state for $\kappa=0.01\chi$, $\kappa=2\chi$, and $\kappa=5\chi$, respectively. The optimal SNR occurs at $\kappa=2\chi$.

$$\text{SNR} = \frac{4n\eta\kappa\chi^2}{\gamma_1(\kappa^2/4 + \chi^2)}. \tag{4.17}$$

A plot of this is shown in Fig. 6. From this plot, it is clear that the optimal value occurs at $\kappa=2\chi$ and is given by $\text{SNR}_{\text{max}}=4n\eta\chi/\gamma_1$.

Thus, to extract the most information about the state of the qubit, we need to tune the measurement drive to bare resonator frequency ω_r and choose the system parameters such that $\chi=\kappa/2$. Note that κ is chosen at fabrication time (and could be tuned *in situ* by a change of resonator design) and that $\chi=g^2/(\omega_a-\omega_r)$ can be tuned *in situ* by tuning ω_a. At a drive strength such that $\bar{n}=n_{\text{crit}}$ [5], the maximum SNR is $\eta\Delta/\gamma_1$, which for current experiments is approximately 50–100. Using the results of Ref. [43], this implies that a measurement fidelity of at least 95% could be achievable in practice. To further increase this value, improvements have to be made to T_1, to minimize the amplifier noise and/or tune the system to be still further in the dispersive regime.

V. MEASUREMENT TIME

In this section, we use the effective SME for the qubit to obtain an estimate for the measurement time. That is, an estimate for how long it takes us to be confident about the state of the qubit. To do so, we will take the simplifying assumption that the resonator transient can be ignored (that is, $\Gamma_d=\Gamma_m/2$). In this situation, the simplest definition for a measurement time is to assume it is the inverse of the information gain rate,

$$t_{\text{m}} = 1/\Gamma_{\text{ci}}. \tag{5.1}$$

Using this definition, we can write

$$t_{\text{m}}\Gamma_{\text{d}} \leq 1/2. \tag{5.2}$$

This is the information-gain–dephasing "uncertainty relation" already discussed by several authors [44–47]. The

equality is saturated for $\eta=1$ and $\phi=\theta_\beta$ and corresponds to the quantum limit discussed in Ref. [46].

In the next sections, we define the measurement time with respect to three different measures. As we will see however, there is no unique definition of the measurement time.

A. Integrated signal

For simplicity, let us first discuss the situation where $\gamma_1 =0$ and with the qubit initially in either $z=\pm 1$. In this situation, the measurement time is very well defined as the qubit state simply remains in its initial state and the task is to estimate that state in the shortest possible time.

We define the measurement signal for an integration time t as

$$s(t) = \sqrt{\Gamma_{\text{ci}}} \int_0^t \bar{J}(t')dt'. \tag{5.3}$$

This signal has mean and standard deviation

$$\bar{s}(t) = \pm t\Gamma_{\text{ci}}, \tag{5.4}$$

$$\Delta|s(t)| = \sqrt{\langle[s(t)-\bar{s}(t)]^2\rangle} = \sqrt{t\Gamma_{\text{ci}}}. \tag{5.5}$$

As a result, if we were to measure the system for a time t and repeat this measurement several times, we would be confident that, to one standard deviation, the value of s is $\pm t\Gamma_{\text{ci}} \pm \sqrt{t\Gamma_{\text{ci}}}$. As a result, to be able to distinguish between $z=\pm 1$ a reasonable requirement is

$$\Delta|s(t)| \leq t\Gamma_{\text{ci}}. \tag{5.6}$$

The equality defines the measurement time to be $t_{\text{m}}=1/\Gamma_{\text{ci}}$. In this case, we recover the simple assumption discussed above.

A problem with this approach is that the condition which defines distinguishability, and thus the measurement time, is somewhat arbitrary. Indeed, separation by one standard deviation is not the only possible choice for distinguishability. Lastly, the above discussion only answers the question of how much time it takes to distinguish between two predetermine initial states of the qubit (under a measurement with Gaussian noise). A more natural question is how long it takes the conditional state to collapse to either $z=\pm 1$. This can be characterized by the conditional variance.

B. Conditional variance

How fast the ensemble of possible trajectories converge to one of the possible values $z=\pm 1$ is characterized by the conditional variance [48]. This measure is defined as

$$V_J(t) = \langle\sigma_z^2\rangle_t - \langle\sigma_z\rangle_t^2 = 1 - z_J(t)^2. \tag{5.7}$$

It ranges from 0 to 1, with $V_J=0$ meaning that we are certain that the current value of $z_J(t)$ is either ± 1 and $V_J=1$ corresponding to complete uncertainty.

For $\gamma_1=0$, Eq. (4.13) can be solved analytically using Itô calculus. Doing this yields the solution

$$z_J(t) = \tanh\{s(t) + \tanh^{-1}[z(0)]\}, \tag{5.8}$$

where the signal $s(t)$ is defined in Eq. (5.3). For example, in the situation where $z(0)=0$ and arbitrary $x(0)$ and $y(0)$ (for
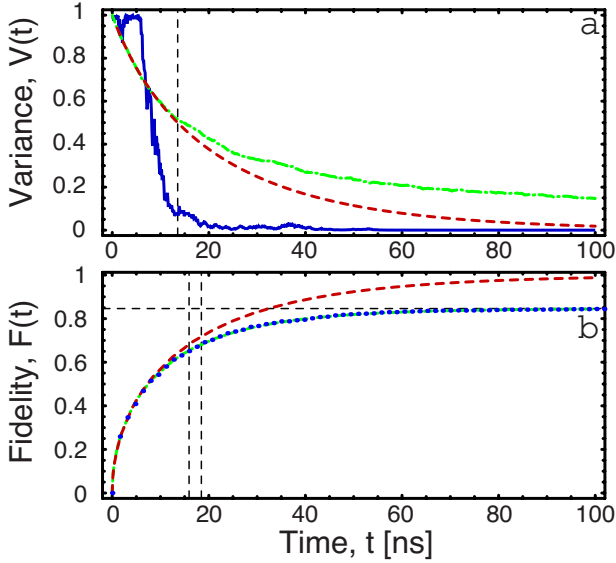
FIG. 7. (Color online) (a) Typical trajectories for the conditional variance (blue solid line) with $\Gamma_d/2\pi=5$ MHz and $\eta=1$. Average conditional variance (red dashed line) found using Eq. (5.10) for the same parameters. Note that the calculated ensemble average over 1000 typical trajectories falls directly over the average conditional variance, and is therefore not explicitly shown. The vertical dash line shows the time at which the conditional variance crosses $1/2$, $t_m=13.5$ ns. The green dashed-dotted line is the ensemble average conditional variance for $T_1=159$ ns ($\gamma_1/2\pi=1$ MHz) and the rest of the parameters identical as above. For this value of γ_1, the SNR is 10. (b) Average fidelity of the measurement at estimating an unknown but pure initial state for $\Gamma_d/2\pi=5$ MHz, $\eta=1$, and $\gamma_1/2\pi=0$ (red dashed line) or $\gamma_1/2\pi=1$ MHz (blue dots). The green solid line is a fit using Eq. (5.18) with fit parameters $A_{fit}=0.846$ (horizontal dashed line) and $\Gamma_{fit}/2\pi=14.6$ MHz. The two vertical lines correspond to the times where the fidelity crosses $\text{erf}(1/\sqrt{2})$. For $\gamma_1/2\pi=0$ this yields $t_m=15.9$ ns, while for $\gamma_1/2\pi=1$ we find $t_m=18.5$ ns.

example, a completely mixed state or an x eigenstate) the conditional variance becomes

$$V_J(t) = 1 - \tanh^2[s(t)]. \qquad (5.9)$$

The conditional variance for a typical trajectory is shown in Fig. 7(a) (blue solid line). Here, we have taken $\Gamma_d/2\pi=5$ MHz and the qubit to be initially completely mixed [$x(0)=y(0)=z(0)=0$]. We see that for this typical trajectory, at about 10 ns the measurement is completed and the state of the qubit is almost pure. However, this is only *one* typical trajectory and to obtain a quantitative idea of the measurement time we must consider the ensemble average of the conditional variance. This is the red dashed line in Fig. 7(a).

Taking the ensemble average of Eq. (5.9) gives

$$V(t) = \frac{1}{2\sqrt{2\pi}\nu^{3/2}} \int_{-\infty}^{\infty} \frac{x \sinh(2x)\exp(-x^2/2\nu)}{\cosh(2\nu) + \cosh(2x)} dx, \qquad (5.10)$$

where $\nu=\Gamma_{ci}t$. Using this, the measurement time t_m can be defined by requiring that the average conditional variance

falls below $1/2$. Numerically, this is found to occur when $\nu=0.851$. Thus, using the conditional variance as the measure, the measurement time is found to be $t_m=0.851/\Gamma_{ci}$.

However, when γ_1 is nonzero, the conditional variance always eventually goes to zero which signifies that we are eventually certain that the system is in its ground state. This is of course not a useful way to define the measurement time. To take into account relaxation, in Ref. [43] we studied this question by considering an effective classical model for a dispersive quantum nondemolition measurement which turns out to be equivalent to the model presented here when the initial state of the qubit is either $z(0)=\pm 1$ or a mixture of both [i.e., $x(0)=y(0)=0$]. That is, Eq. (4.13) is the same as the Kushner-Stratonovich equation that describes a measurement of a two state system with Gaussian noise. For completeness and since this is a good approach in the situation where relaxation is nonzero, we will therefore briefly review the relevant results of Ref. [43].

C. Initial state fidelity

In Ref. [43], to quantify how good a measurement is at revealing the initial state of the qubit, we imagine preparing the qubit in either the $z(0)=\pm 1$ state and then generate fictitious records $\bar{J}(t)$ from that input. Given these fictitious measurement records, but now assuming ignorance of the initial state, we then ask what was the initial state of the qubit. To quantify the efficiency of the measurement at revealing the correct input state, we use the following fidelity measure F: the number of correct assignments minus the number of incorrect assignments of the initial state, normalized by the total number of assignments. This measure will range from 1, indicating that the correct initial state was correctly found for each record, to -1, indicating that a wrong assigned was realized for each record. A fidelity of 0 implies that the assignments are completely random.

The criteria used to make these assignments is the optimal assignment criteria found in Ref. [43]. This is based on an estimate $\tilde{z}(t)$ for the initial state. If this estimate is above 0, we assign the initial state as excited and if it is below 0 we assign it as ground (for $\tilde{z}=0$, we randomly chose between excited or ground). This estimate $\tilde{z}(t)$ is defined as

$$\tilde{z}(t) = P(z_0 = +1|\bar{J},t) - P(z_0 = -1|\bar{J},t), \qquad (5.11)$$

where $P(z_0=\pm 1|\bar{J},t)$ is the probability at time t that the initial state was ± 1 given the record $\bar{J}(t)$. This conditional probability is given by Bayes theorem

$$P(z_0|\bar{J},t) = \frac{P(\bar{J}|z_0,t)P(z_0)}{\sum\limits_{i=-1,1} P(\bar{J}|z_0=i,t)P(z_0=i)}, \qquad (5.12)$$

where $P(z_0)$ is the initial state probability which we take to be $1/2$ for both $i=-1$ and 1. By introducing a fictitious unraveling of γ_1 (see Refs. [39,43]), the estimate can be rewritten as

$$\widetilde{z}(t) = \frac{1 - e^{-2s(t)}[1 - a(t)]}{1 + e^{-2s(t)}[1 + a(t)]}, \tag{5.13}$$

where

$$a(t) = \gamma_1 \int_0^t dt_j e^{-\gamma_1(t_j - t) + 2s(t_j)} \tag{5.14}$$

and $s(t)$ is the integrated signal defined in Eq. (5.3).

The above integral cannot be solved in general for a typical record $s(t)$, but it can be easily determined numerically. Here, however, to develop a physical understanding of this result, we will consider the $\gamma_1 = 0$ limit first. Doing this, we can rewrite $\widetilde{z}(t)$ as

$$\widetilde{z}(t) = \frac{1 - e^{-2s(t)}}{1 + e^{-2s(t)}}, \tag{5.15}$$

and using the above definition of the fidelity

$$F(t) = \lim_{M \to \infty} \frac{1}{2M} \left(\sum_{\widetilde{z}_{+1} > 0} - \sum_{\widetilde{z}_{+1} < 0} + \sum_{\widetilde{z}_{-1} < 0} - \sum_{\widetilde{z}_{-1} > 0} \right) 1, \tag{5.16}$$

we obtain the following compact expression:

$$F(t) = \frac{1}{\sqrt{2\pi t}} \left(\int_{-t\sqrt{\Gamma_{ci}}}^{\infty} e^{-x^2/2t} dx - \int_{-\infty}^{-t\sqrt{\Gamma_{ci}}} e^{-x^2/2t} dx \right)$$

$$= \mathrm{erf}\left(\sqrt{\frac{t\Gamma_{ci}}{2}} \right). \tag{5.17}$$

This result is shown in Fig. 7(b), for $\Gamma_d/2\pi = 5$ MHz, as the red dashed line. As can be seen from this figure, arbitrarily large fidelities can be achieved by monitoring longer.

We now use this result to define a measurement time. A reasonable criterion is to ask for the fidelity to be at least $\mathrm{erf}(1/\sqrt{2}) = 0.68$ (corresponding to the probability of a Gaussian random variable being within one standard deviation of the mean). The measurement time is then defined as the time when the fidelity reaches this value. Using the above results, we find that the measurement time is $t_m = 1/\Gamma_{ci}$. For $\gamma_1 = 0$, we thus again recover the result, Eq. (5.1), of the simple model.

The effect of relaxation on the fidelity is investigated numerically. For example, the blue dots in Fig. 7(b) show the fidelity obtained numerically for $\gamma_1/2\pi = 1$ MHz. With all values of Γ_d tried numerically, we have found excellent agreement of the fidelity, including dissipation, to the following form:

$$F(t) = A_{fit} \, \mathrm{erf}\left(\sqrt{\frac{t\Gamma_{fit}}{2}} \right), \tag{5.18}$$

where Γ_{fit} and A_{fit} are fit parameters. For example, the green solid line in Fig. 7(b) is for $\Gamma_d/2\pi = 5$ MHz. To show how the fidelity $F(t)$ depends on the SNR (which in the limit that the resonator transient can be ignored is $2\Gamma_d/\gamma_1$), numerical simulations and the above described fitting procedure were performed for values of $\Gamma_d/2\pi$ ranging from 1 to 50 MHz. The results of these simulations are shown in Fig. 8. In par-
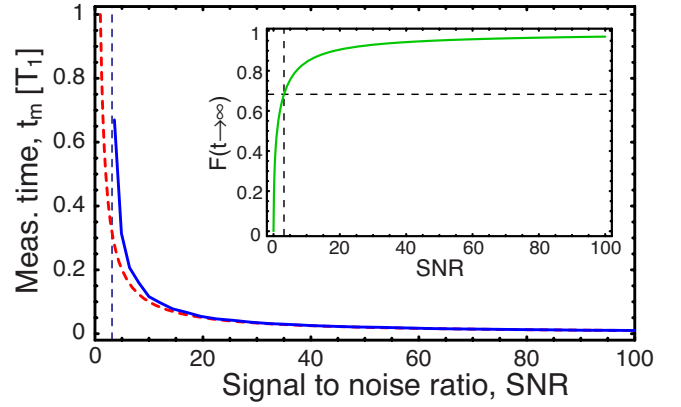

FIG. 8. (Color online) Measurement time (full blue line) as extracted from the requirement that the fidelity reaches $\mathrm{erf}(1/\sqrt{2})$ as a function of the SNR $(2\Gamma_d/\gamma_1)$. This is plotted for $\gamma_1/2\pi = 1$ MHz. The vertical dashed line corresponds to SNR=3.16. This defines the minimal SNR for which we can define a measurement time. This is also presented in the inset which shows the long time fidelity as a function SNR, with the vertical dashed line being the SNR where the long time fidelity crosses $\mathrm{erf}(1/\sqrt{2})$. The red dashed line in the main panel corresponds $t_m = 1/\Gamma_{ci}$, the measurement time for $\gamma_1 = 0$. At low SNR, it always underestimate the measurement time.

ticular, the inset of this figure shows the long time fidelity, A_{fit}. From this result, we see that the fidelity is below $\mathrm{erf}(1/\sqrt{2})$ until a SNR of 3.16 is reached (this corresponds to the vertical dashed line). Below this value, using the above measurement time criteria, we must conclude that the measurement cannot be completed. However, for all SNR above 3.16 it is possible to find a time where the fidelity crosses $\mathrm{erf}(1/\sqrt{2})$. This time is shown in Fig. 8 as the blue solid line. We see that this time is always longer than the ideal limit (red dashed line). However, as the SNR increases, the measurement time approaches the result obtained in the $\gamma_1 = 0$ case $(1/\Gamma_{ci})$.

VI. EMERGENCE OF QUANTUM JUMPS

By increasing the SNR (e.g., increasing the measurement drive amplitude), the conditional state will tend to be localized to either the excited or ground state. This is due to the term $\sqrt{\Gamma_{ci}}(1 - z_J^2)$ in Eq. (4.13). However, in the presence of relaxation $\gamma_1 \neq 0$, on average the conditional state must be localized on the ground state in the long time limit. As a result, when initializing the system in the excited state, there are two competing processes. One is trying to lower the conditional state to $z = -1$ (γ_1) and the second is trying to hold it in at $z = +1$ (Γ_{ci}). The net result is that as the measurement strength becomes stronger, the SME will transform from a diffusive stochastic process which stochastically lowers itself to the ground state to one which jumps at a well-defined time. That is, as the measurement becomes stronger, quantum jumps due to the decay channel γ_1 will be revealed in the signal $J(t)$.

The crossover of the conditional state from a diffusive to jumplike SME is numerically shown in Fig. 9 for measure-
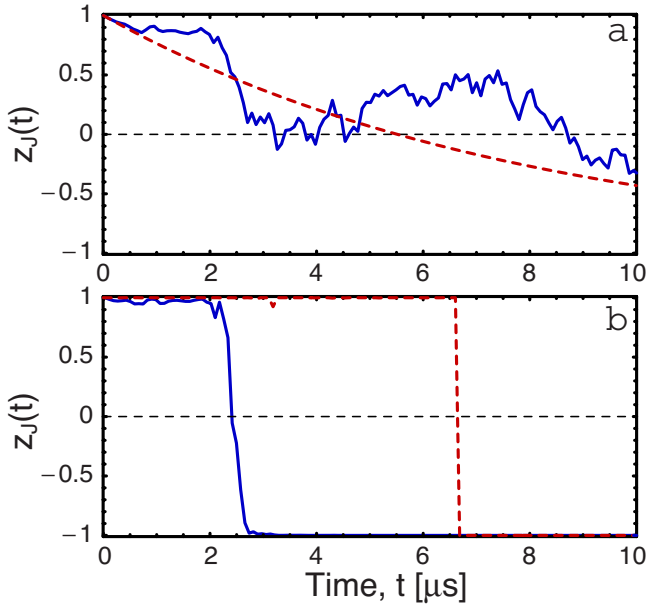
FIG. 9. (Color online) Time evolution of the z component of the conditional state for a qubit initially in the excited state and $\chi/2\pi$ =5 MHz, $\kappa/2\pi$=10 MHz, Δ_r=0, η=1, and T_1=7 μs. (a) Measurement drive strength of $\varepsilon_d/2\pi$=0 MHz (red dashed line) and 0.2 MHz (solid blue line). (b) $\varepsilon_d/2\pi$=0.9 MHz (solid blue line) and 20 MHz (dashed red line).

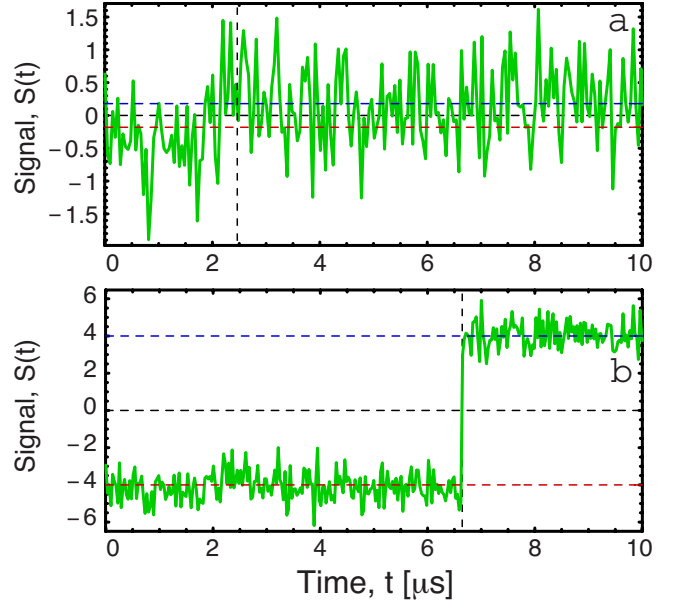FIG. 10. (Color online) Integrated signal $S(t)$ as a function of time. (a) Measurement drive strength $\varepsilon_d/2\pi$=0.9 MHz and integration steps δt=48 ns. (b) $\varepsilon_d/2\pi$=20 MHz and δt=32 ns. The vertical dashed line indicates the time where the conditional state crosses 0 in Fig. 9. The two horizontal dashed lines are the expected results corresponding to $z=\pm 1$ constant.

ment drive strengths $\varepsilon_d/2\pi=\{0,0.2,0.9,20\}$ MHz, respectively. From this figure, we see that when $\varepsilon_d/2\pi$=0 [dashed red line in Fig. 9(a)], as expected, the state simply decays to the ground state at a rate γ_1 as this is equivalent to gaining no information about the qubit state. For $\varepsilon_d/2\pi$=0.2 MHz [full blue line in Fig. 9(a)] it stochastically follows this decay curve. However, at $\varepsilon_d/2\pi$=0.9 MHz [full blue line in Fig. 9(b)], there appears a sharp transition from the excited state to the ground state. As the measurement amplitude is further increased [$\varepsilon_d/2\pi$=20 MHz, red dashed line in Fig. 9(b)], this transition becomes sharper and happens at a well-defined time.

Experimentally, one does not have direct access to $z_J(t)$ but reconstructs this quantity from the measured current $J(t)$. As a result, a more striking demonstration of quantum jumps would be to see these jumps directly in $J(t)$. However, due to white noise fluctuations $\xi(t)$, without first averaging the signal over some finite integration time the jumps are not visible in most trajectories. As a result, we consider the quantity

$$S(t) = \frac{1}{\delta t}\int_t^{t+\delta t} \frac{J(s)}{\sqrt{\kappa\eta}}ds, \tag{6.1}$$

where δt is an adjustable integration parameter. At large δt, the fluctuations are well suppressed by the averaging, but at the expense of smoothing out the jump. For example, Fig. 10 shows the integrated current corresponding to the two measurement amplitudes used in Fig. 9(b). Figure 10(a) corresponds to $\varepsilon_d/2\pi$=0.9 MHz and δt=48 ns, while Fig. 10(b) corresponds to $\varepsilon_d/2\pi$=20 MHz and δt=32 ns. From this figure, we see that for $\varepsilon_d/2\pi$=0.9 MHz one cannot resolve the

jump from the integrated signal. However, by increasing the drive to $\varepsilon_d/2\pi$=20 MHz the jump becomes clearly visible.

Thus we see that if we wish to see the jump in the integrated signal we need a much higher signal to noise ratio. This is because by definition the conditional state is the best way we can process the record. We note that it should be possible to optimize the processing of the current to distinguish the jump at lower SNR by using a more complicated filter then time averaging. For example, one could easy envisage that there exists an optimal integration time $\delta t = t_{\text{opt}}$, or kernel $k(t)$, such that the integrated signal, $S(t)$ $=\int_{-\infty}^{\infty}k(t,s)J(s)dt$, would do almost as well as the conditional state (see Ref. [43] where a similar question was investigated).

Finally, an interesting situation occurs if the γ_1 channel can be directed (corresponding to fluorescence of the "atom"). When we register that the qubit has jumped, we know that the energy has been dissipated into the γ_1 channel. If this fluorescence is directed to an additional low-Q resonator, this can be used as a single microwave photon source with a well-defined emission time. Inversely, if the qubit is prepared in the ground state this second resonator can be used as a single photon dector. When a jumped of the qubit is registered, we know that photon was present in the second cavity. The efficiency of this detector will be limited by the Zeno effect [49].

VII. WEAK DRIVING OF THE QUBIT—ZENO EFFECT

In the previous sections, we considered the dynamics of the qubit under measurement. In this section, we will include

the possibility of having a control drive. As explained in Sec. II, this is done in practice by adding a drive on the input port of the resonator at the qubit transition frequency. Our goal is to use the transformation, Eq. (3.8), to again obtain an effective SME for the qubit only. However, as shown in Appendix C, in the transformed frame, the drive on the qubit induces transitions between the different (transformed) states of the resonator. As a result, it is not possible to integrate out exactly the resonator from the effective description of the qubit.

However, in the small β limit, we find that qubit evolution is well described by the SME,

$$\dot{\rho_{\bar{J}}}(t) = -i\frac{\Omega_R}{2}[\sigma_x, \rho_{\bar{J}}(t)] + [\gamma_\phi + \Gamma_d(t)]\mathcal{D}[\sigma_z]\rho_{\bar{J}}(t)/2$$

$$-i\frac{\sqrt{\Gamma_{ba}}}{2}[\sigma_z, \rho_{\bar{J}}(t)](\bar{J}(t) - \sqrt{\Gamma_{ci}}\langle\sigma_z\rangle_t) + \sqrt{\Gamma_{ci}}\mathcal{M}[\sigma_z]\rho_{\bar{J}}(t)$$

$$\times(\bar{J}(t) - \sqrt{\Gamma_{ci}}\langle\sigma_z\rangle_t) + \gamma_1\mathcal{D}[\sigma_-]\rho_{\bar{J}}(t), \qquad (7.1)$$

where Ω_R is the Rabi frequency of the control drive tuned to the qubit frequency, ω_{ac}. The competition between Rabi flopping induced by the control drive and the extra dephasing due to the measurement drive should enable us to observe the Zeno effect in this system. Indeed, as the measurement rate Γ_{ci} is increased, the qubit dynamics will switch from Rabi oscillations to jumplike behavior. In the limit of very large measurement rates, all dynamics will disappear and the qubit will remain fixed in the $z_J = \pm 1$ state (if γ_1 is zero).

To see this more clearly, the above SME can be written in terms of the components of the Bloch vectors as

$$\dot{x_J}(t) = -\{\gamma_2 + \Gamma_d(t) + \sqrt{\Gamma_{ci}}z_J(t)[\bar{J}(t) - \sqrt{\Gamma_{ci}}z_J(t)]\}x_J(t),$$

$$\dot{y_J}(t) = -\Omega_R z_J(t) - \{\gamma_2 + \Gamma_d(t) + \sqrt{\Gamma_{ci}}z_J(t)$$

$$\times[\bar{J}(t) - \sqrt{\Gamma_{ci}}z_J(t)]\}y_J(t),$$

$$\dot{z_J}(t) = \Omega_R y_J(t) - \gamma_1[z_J(t) + 1] + \sqrt{\Gamma_{ci}}[1 - z_J(t)^2]$$

$$\times[\bar{J}(t) - \sqrt{\Gamma_{ci}}z_J(t)]. \qquad (7.2)$$

Here we have assumed that $\phi = \theta_\beta$ such that $\Gamma_{ba} = 0$. In the limit that the measurement-induced dephasing rate Γ_d is much larger than all other rates, we can set $\dot{x_J}(t) = \dot{y_J}(t) = 0$ to arrive at

$$\dot{z_J}(t) = -2\gamma_{jump}z_J(t) - \gamma_1[z_J(t) + 1]$$

$$+ \sqrt{\Gamma_{ci}}[1 - z_J(t)^2][\bar{J}(t) - \sqrt{\Gamma_{ci}}z_J(t)]. \qquad (7.3)$$

As expected, in this expression, the jump rate is given by $\gamma_{jump} = \Omega_R^2/2(\gamma_2 + \Gamma_d)$. From this expression, we can indeed expect Zeno-type dynamics for the qubit. Note that the stochastic term $\sqrt{\Gamma_{ci}}z_J(t)[\bar{J}(t) - \sqrt{\Gamma_{ci}}z_J(t)]$ has been ignored in the denominator of the jump rate.

As discussed in Sec. VI, as the measurement becomes stronger (i.e., Γ_{ci} increases) the conditional state will lock itself into either the excited or ground state ($z = \pm 1$). Because of the control drive, whose amplitude enters in the jump rate γ_{jump}, random fluctuations will result in the system
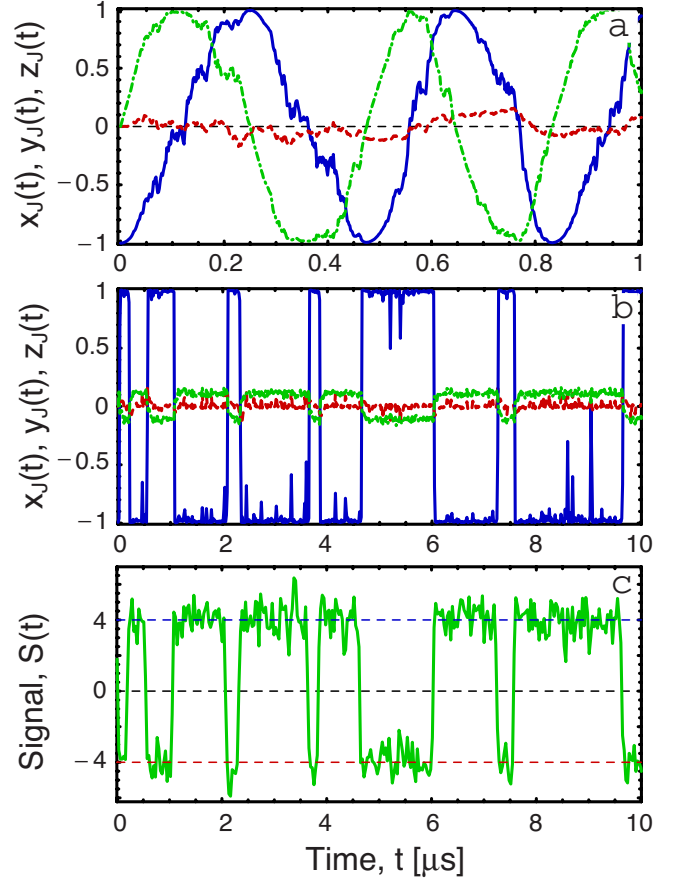

FIG. 11. (Color online) Time evolution of the conditional state for the full homodyne SME for a qubit initially in the ground state: x, red dashed line; y, green dashed-dotted line; z, solid blue line. The system parameters are $\chi/2\pi = 5$ MHz, $\kappa/2\pi = 10$ MHz, $\Delta_r = 0$, $\eta = 1$, $\gamma_1 = \gamma_\phi = 0$, and $\Omega_R/2\pi = 2.5$ MHz. (a) Measurement drive amplitude of $\varepsilon_d/2\pi = 0.9$ MHz. (b) $\varepsilon_d/2\pi = 20$ MHz. (c) Integrated signal with $\delta t = 32$ ns and for a measurement amplitude of $\varepsilon_d/2\pi = 20$ MHz.

jumping between these two localized states. However, unlike the situation presented in the previous section, the rate of these jumps also depends on the measurement strength through Γ_{ci}. As a result, in the limit that the measurement SNR is large, the jumps will disappear and the qubit will remain fixed in either $z = \pm 1$. This is the Zeno effect [24–27].

To illustrate this, we have numerically integrated the full homodyne SME (4.2), with the addition of a qubit drive, for two different measurement drives $\varepsilon_d/2\pi = 0.9$ MHz and 20 MHz, and a Rabi frequency of $\Omega_R/2\pi = 2.5$ MHz. The results are shown in Fig. 11. From this figure, we see that for the low measurement amplitude [Fig. 11(a)], measurement only causes small amplitude noise on the Rabi oscillations. However, for the larger amplitude [Fig. 11(b)] the conditional dynamics is jumplike. We note that the rate of the jumps between the ground and excited state is, as expected from the above discussion, slower then the rate Ω_R at which the Rabi drive would coherently drive the system. Note that the x-axis scale is not the same in Fig. 11(a) and Fig. 11(b) [Fig. 11(c)].
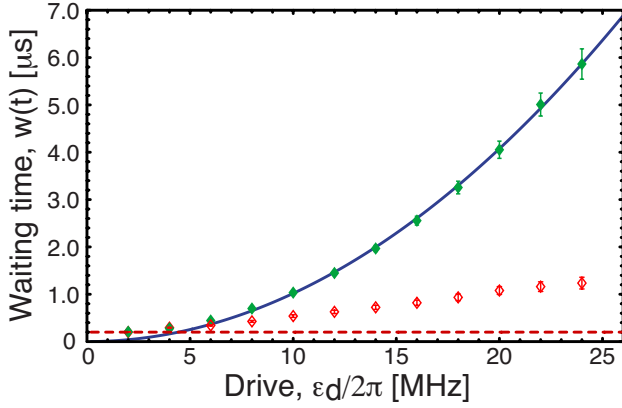
FIG. 12. (Color online) Average jump time as a function of the measurement drive strength ε_d. The jump time is defined as the time for the system state to go from $z = \pm 0.95$ to $z = \mp 0.95$. The red dashed line corresponds to the Rabi period π/Ω_R of 200 ns for a Rabi drive of $\Omega_R/2\pi = 2.5$ MHz. The blue solid line corresponds to the expected mean jump time expected from the Zeno effect, $\gamma_{jump} = \Omega_R^2/2(\gamma_2 + \Gamma_d)$. This agrees very well with the numerically simulations of Eq. (7.1) (green filled diamonds) where the mean jump time was extracted from a total simulation time of 16 ms. The red open diamonds are the mean jump time as extracted from the full numerical homodyne SME for a total simulation time of about 15 ms.

These jumps can be observed directly in the signal $J(t)$. This is illustrated in Fig. 11(c) for the case of the larger measurement amplitude. As in the previous section, we are showing here the integrated signal, defined in Eq. (6.1), and with a integration time $\delta t = 32$ ns. The integrated signal clearly reveals the jumps.

We note that the numerical results presented here were obtained using the full homodyne SME, and not the simplified SME (7.1). This is because while this simplified equation contains the essential features, it is not strictly valid in the limit of large mean photon number. However, by inspecting individual trajectories, we find that trajectories obtained from the full model display the same qualitative behavior as those obtained from the effective model. The difference between the two types of trajectories appear to be only small changes in renormalized system parameters.

To explore the difference between these two models in more detail, we simulated both models as a function of the measurement drive strength ε_d. The average jump time extracted for both cases is shown in Fig. 12. The simple model (green filled diamonds) agrees with the predicted jump time $1/\gamma_{jump}$ for large ε_d (blue solid line). In the low measurement drive limit, it agrees with the time set by the Rabi drive (red dashed line). However, the full homodyne SME calculations (red open diamonds) do not agree with this expectation in the large drive case. Although the mean jump time does increase with the measurement drive as expected by the Zeno effect, its effect is not as large as that predicted by the simple model.

VIII. CONCLUSION

We have investigated the measurement of a superconducting qubit using a dispersively coupled resonator. From the fully quantum mechanical model for the resonator and qubit dispersive interaction, we have found an effective master equation for the qubit (only) under the presence of a measurement drive on the resonator. This was done by moving to a frame which takes into account the entanglement between the resonator and the qubit. With respect to the bare qubit-resonator master equation, the effective qubit master equation contains an additional, time-dependent decay channel which has the form of a dephasing process and which depends on the number of photons populating the resonator. This is referred to as measurement-induced dephasing [9,44–47]. In addition to the extra dephasing channel, the photon population of the resonator is also responsible for an ac-Stark shift of the qubit transition frequency. As was shown in Refs. [9,22], and later reported experimentally in Ref. [23], these effects lead to *number splitting* of the qubit spectrum in the limit where $\chi \gg \kappa$. We thus have obtained a very simple to solve (two-dimensional Hilbert space) effective model for the qubit dynamics that contains the essential physics. We believe that this is an interesting analytical, and numerical, tool to further explore the dispersive regime.

We then focused on the situation where one is continuously monitoring the voltage at the output port of the resonator. In that situation, the conditional state of the combined system evolves according to the homodyne SME [12]. Again moving to a frame that takes into account the qubit-resonator entanglement, we then obtained an effective SME for the qubit that is valid in the limit $\gamma_1 \ll \kappa$. The SME corresponds to a weak measurement of the qubit operator σ_z. As a result, the measurement stochastically projects the conditional state into eigenstates of σ_z. This is similar to the result that was obtained in Refs. [13–20] for a double quantum dot qubit monitored continuously by a quantum point contact (although the results are presented in very different forms in all of these references).

From these results, we then showed how, in the limit that the measurement becomes strong, there is a crossover in the qualitative behavior of the trajectories from diffusive to jumplike. This process relies on the T_1 decay channel for the qubit to jump from the excited to the ground state. As a result, we expect to see quantum jumps, with Poisson statistics, in the measured homodyne current.

Moreover, in presence of a Rabi drive on the qubit, we again saw that the trajectories evolve from diffusive to jumplike. In this situation and when the measurement drive is not too strong, the jump rate is given $\Omega_R^2/2(\gamma_2 + \Gamma_d)$. This is due to a competition between the measurement drive that tends to lock the conditional state on one of the eigenstates of σ_z and the Rabi drive that tends to flip the qubit. This is nothing but the Zeno effect. However, as the measurement becomes stronger, the simple dispersive Hamiltonian approximation breaks down and the effective model fails to predict the correct mean jump time for the qubit. We found that the form of the trajectories are still consistant with the model, only the parameters appear to be renormalized by the stronger measurement drive. An interpretation of this discrepancy is that the resonator response is not instantaneous. When the qubit jumps, the resonator state will lag behind and as a result the effective separation in phase space between the two coherent states of the resonator corresponding to the two qubit states

will be reduced. In turn, this can lead to a reduction of the measurement-induced dephasing.

Overall, the model obtained here can be used to obtain qualitative information about the qubit dynamics in the presence of dissipation, measurement, and control. We also gave a numerical prescription to go beyond this simple model.

APPENDIX A: DERIVATION OF THE EFFECTIVE QUBIT MASTER EQUATION

In this appendix we show how to obtain the effective qubit master equation, Eq. (3.10), from the full dispersive qubit-resonator master equation, Eq. (3.1). For this purpose, we introduce the the transformation

$$\mathbf{P} = \Pi_e D(\alpha_e) + \Pi_g D(\alpha_g), \tag{A1}$$

where $\Pi_{e,g}$ are the projectors on the qubit excited and ground state and $D(\alpha)$ is the field displacement operator [50].

In this frame, the state of the combined qubit-resonator system $\varrho^{\mathbf{P}} = \mathbf{P}^\dagger \varrho \mathbf{P}$ can be written in the energy basis as

$$\varrho^{\mathbf{P}} = \sum_{n,m=0}^{\infty} \sum_{i,j=e,g} \varrho^{\mathbf{P}}_{n,m,i,j} |n,i\rangle\langle m,j|. \tag{A2}$$

Using this expression for the system's density matrix in the transformed frame, it is simple to express the qubit's reduced density matrix in laboratory frame as

$$\rho = \mathrm{Tr}_{\mathrm{res}}[\mathbf{P}\varrho^{\mathbf{P}}\mathbf{P}^\dagger] = \sum_n [\varrho^{\mathbf{P}}_{n,n,e,e}|e\rangle\langle e| + \varrho^{\mathbf{P}}_{n,n,g,g}|g\rangle\langle g|]$$
$$+ \sum_{n,m} [\lambda_{n,m,m,n}|e\rangle\langle g| + \lambda^{*}_{m,n,n,m}|g\rangle\langle e|] \tag{A3}$$

with

$$\lambda_{n,m,p,q} = \varrho^{\mathbf{P}}_{n,m,e,g} d_{p,q} \exp(-i \, \mathrm{Im}[\alpha_g \alpha^{*}_e]) \tag{A4}$$

and $d_{p,q}$ is the matrix element of the displacement operator in the photon number basis

$$d_{p,q} = \langle p|D(\beta)|q\rangle. \tag{A5}$$

In the remainder of this appendix, we show how by using the transformed master equation for $\varrho^{\mathbf{P}}$ it is possible to obtain the coefficients entering in Eq. (A3) for ρ.

1. The displaced frame

In the displaced frame, the state matrix $\varrho^{\mathbf{P}}$ obeys the master equation

$$\dot{\varrho}^{\mathbf{P}} = -\frac{i}{\hbar}[H^{\mathbf{P}}_{\mathrm{eff}}, \varrho^{\mathbf{P}}] + \kappa\mathcal{D}[a^{\mathbf{P}}]\varrho^{\mathbf{P}} + \gamma_1\mathcal{D}[\sigma^{\mathbf{P}}_-]\varrho^{\mathbf{P}}$$
$$+ \gamma_\phi\mathcal{D}[\sigma^{\mathbf{P}}_z]\varrho^{\mathbf{P}}/2 - \mathbf{P}^\dagger\dot{\mathbf{P}}\varrho^{\mathbf{P}} - \varrho^{\mathbf{P}}\dot{\mathbf{P}}^\dagger\mathbf{P}, \tag{A6}$$

with $O^{\mathbf{P}} = \mathbf{P}^\dagger O \mathbf{P}$ the transformed operators and where the effective Hamiltonian H_{eff} is given by Eq. (2.2). Using the standard results

$$D^\dagger(\alpha)aD(\alpha) = a + \alpha, \quad D^\dagger(\alpha)a^\dagger D(\alpha) = a^\dagger + \alpha^*, \tag{A7}$$

we obtain

$$a^{\mathbf{P}} = a + \Pi_\alpha,$$

$$(a^\dagger a)^{\mathbf{P}} = a^\dagger a + a^\dagger \Pi_\alpha + a\Pi^{*}_\alpha + |\alpha_g|^2\Pi_g + |\alpha_e|^2\Pi_e, \tag{A8}$$

where we have defined

$$\Pi_\alpha = \alpha_g\Pi_g + \alpha_e\Pi_e. \tag{A9}$$

For the qubit operators, we obtain

$$\sigma^{\mathbf{P}}_z = \sigma_z, \quad \sigma^{\mathbf{P}}_- = \sigma_- D^\dagger(\alpha_g)D(\alpha_e). \tag{A10}$$

Using these results, we then have for the transformed Hamiltonian

$$H^{\mathbf{P}}_{\mathrm{eff}} = \frac{\hbar\widetilde{\omega}_a}{2}\sigma_z + \hbar[\varepsilon_d(a^\dagger + \Pi^{*}_\alpha) + \mathrm{H.c.}]$$
$$+ \hbar(\Delta_r + \chi\sigma_z)(a^\dagger a + a^\dagger\Pi_\alpha + a\Pi^{*}_\alpha + |\Pi_\alpha|^2). \tag{A11}$$

We now turn to the damping superoperators. For the field damping, we find

$$D[a^{\mathbf{P}}]\varrho^{\mathbf{P}} = D[a]\varrho^{\mathbf{P}} - \frac{1}{2}[a^\dagger\Pi_\alpha - a\Pi^{*}_\alpha, \varrho^{\mathbf{P}}] + \frac{\beta^*}{2}a[\varrho^{\mathbf{P}}, \sigma_z]$$
$$+ \frac{\beta}{2}[\sigma_z, \varrho^{\mathbf{P}}]a^\dagger + \frac{\Gamma_{\mathrm{m}}(t)}{4\kappa}\mathcal{D}[\sigma_z]\varrho^{\mathbf{P}}$$
$$- i\frac{\mathrm{Im}[\alpha_g\alpha^{*}_e]}{2}[\sigma_z, \varrho^{\mathbf{P}}], \tag{A12}$$

where

$$\Gamma_{\mathrm{m}} = \kappa|\beta|^2 \tag{A13}$$

and

$$\beta = \alpha_e - \alpha_g. \tag{A14}$$

In this frame, damping of the field induces extra dephasing of the qubit at a rate Γ_{m}. Note this is not the measurement-induced dephasing rate given in Ref. [9], as the present expressions are in the transformed frame, not the laboratory frame. Transforming the qubit dissipation superoperators, we obtain

$$\mathcal{D}[\sigma^{\mathbf{P}}_z]\varrho^{\mathbf{P}} = \mathcal{D}[\sigma_z]\varrho^{\mathbf{P}}, \tag{A15}$$

$$\mathcal{D}[\sigma_-^{\mathbf{P}}]\varrho^{\mathbf{P}} = \mathcal{D}[\sigma_- D^\dagger(\alpha_g)D(\alpha_e)]\varrho^{\mathbf{P}}. \quad (A16)$$

The last terms to take into account are those in the last line of Eq. (A6). For these terms, we use the fact that

$$\dot{D}(\alpha) = [(\dot{\alpha}a^\dagger - \dot{\alpha}^*a) + (\dot{\alpha}^*\alpha - \dot{\alpha}\alpha^*)/2]D(\alpha) \quad (A17)$$

to obtain

$$-\mathbf{P}^\dagger\dot{\mathbf{P}}\varrho^{\mathbf{P}} - \varrho^{\mathbf{P}}\mathbf{P}^\dagger\dot{\mathbf{P}} = -[\dot{\Pi}_\alpha a^\dagger - \dot{\Pi}_\alpha^*a, \varrho^{\mathbf{P}}] - i[\mathrm{Im}[\dot{\alpha}_e\alpha_e^*]\Pi_e$$
$$+ \mathrm{Im}[\dot{\alpha}_g\alpha_g^*]\Pi_g, \varrho^{\mathbf{P}}]. \quad (A18)$$

Choosing $\dot{\alpha}_e$ and $\dot{\alpha}_g$ in the above expression as in Eq. (3.5), we finally obtain the transformed master equation

$$\varrho^{\mathbf{P}} = -i\frac{\widetilde{\omega}_a + \widetilde{B}}{2}[\sigma_z, \varrho^{\mathbf{P}}] - i[(\Delta_r + \chi\sigma_z)a^\dagger a, \varrho^{\mathbf{P}}]$$
$$+ \gamma_1\mathcal{D}[\sigma_- D^\dagger(\alpha_g)D(\alpha_e)]\varrho^{\mathbf{P}} + [\gamma_\phi + \Gamma_m/2]\mathcal{D}[\sigma_z]\varrho^{\mathbf{P}}/2$$
$$+ \kappa\mathcal{D}[a]\varrho^{\mathbf{P}} + \frac{\kappa\beta}{2}[\sigma_z, \varrho^{\mathbf{P}}]a^\dagger + \frac{\kappa\beta^*}{2}a[\varrho^{\mathbf{P}}, \sigma_z], \quad (A19)$$

where we have defined the time-dependent shifted qubit transition frequency as

$$\widetilde{B} = (\beta\varepsilon_d^* + \beta^*\varepsilon_d)/2 + \kappa\,\mathrm{Im}[\alpha_g\alpha_e^*]. \quad (A20)$$

In this transformed frame, the last two terms of Eq. (A19) appear because the resonator acts as a non-Markovian bath for the qubit [51,52]. Moreover, we note that the term proportional to γ_1 in Eq. (A19) can be expressed as

$$\mathcal{D}[\sigma_- D^\dagger(\alpha_g)D(\alpha_e)]\varrho^{\mathbf{P}}$$
$$= \sigma_- D(\beta)\varrho^{\mathbf{P}}\sigma_+ D^\dagger(\beta) - \sigma_+\sigma_-\varrho^{\mathbf{P}}/2 - \varrho^{\mathbf{P}}\sigma_+\sigma_-/2. \quad (A21)$$

Upon taking the trace over the resonator space, this expression will simply take the form of regular Markovian γ_1 damping on the qubit. This is one of the features of the transformed master equation that will allow us, below, to obtain a simple effective master equation for the qubit only.

2. Moving back to the laboratory frame

Using Eqs. (A2) and (A19), we obtain the following set of coupled differential equations for the coefficients of the laboratory frame reduced qubit density matrix, Eq. (A3):

$$\dot{\varrho}_{n,m,e,e}^{\mathbf{P}} = [-i\Delta_r(n-m) - i\chi(n-m) - \gamma_1 - \kappa(n+m)/2]\varrho_{n,m,e,e}^{\mathbf{P}}$$
$$+ \kappa\varrho_{n+1,m+1,e,e}^{\mathbf{P}}\sqrt{(n+1)(m+1)}, \quad (A22)$$

$$\dot{\varrho}_{n,m,g,g}^{\mathbf{P}} = [-i\Delta_r(n-m) + i\chi(n-m) - \kappa(n+m)/2]\varrho_{n,m,g,g}^{\mathbf{P}}$$
$$+ \gamma_1\sum_{p,q}\varrho_{p,q,e,e}^{\mathbf{P}}d_{n,p}d_{m,q}^*$$
$$+ \kappa\varrho_{n+1,m+1,g,g}^{\mathbf{P}}\sqrt{(n+1)(m+1)}, \quad (A23)$$

$$\dot{\lambda}_{n,m,p,q} = \varrho_{n,m,e,g}^{\mathbf{P}}d_{p,q}e^{-i\,\mathrm{Im}[\alpha_g\alpha_e^*]} - i\partial_t(\mathrm{Im}[\alpha_g\alpha_e^*])\lambda_{n,m,p,q}$$
$$+ \dot{\beta}\sqrt{p}\lambda_{n,m,p-1,q} - \dot{\beta}^*\sqrt{q}\lambda_{n,m,p,q-1} - \frac{1}{2}\partial_t(\beta\beta^*)\lambda_{n,m,p,q}$$
$$\quad (A24)$$

$$= [-i(\widetilde{\omega}_a + B) - i\Delta_r(n-m) - i\chi(n+m)$$
$$- \gamma_1/2 - \gamma_\phi - \Gamma_d - \kappa(n+m)/2]\lambda_{n,m,p,q}$$
$$+ \kappa\lambda_{n+1,m+1,p,q}\sqrt{(n+1)(m+1)} + \kappa\beta\sqrt{m+1}\lambda_{n,m+1,p,q}$$
$$- \kappa\beta^*\sqrt{n+1}\lambda_{n+1,m,p,q} + \dot{\beta}\sqrt{p}\lambda_{n,m,p-1,q}$$
$$- \dot{\beta}^*\sqrt{q}\lambda_{n,m,p,q-1}, \quad (A25)$$

where Eq. (A24) was obtained by differentiating Eq. (A4), with respect to time and

$$\Gamma_d = 2\chi\,\mathrm{Im}[\alpha_g\alpha_e^*] \quad (A26)$$

and

$$B = 2\chi\,\mathrm{Re}[\alpha_g\alpha_e^*]. \quad (A27)$$

To reconstruct the effective master equation from these amplitudes, we note that the time derivative of the $|e\rangle\langle e|$ component of Eq. (A3) can be written as

$$\dot{\rho}_{e,e} = \sum_n\dot{\varrho}_{n,n,e,e}^{\mathbf{P}} = -\gamma_1\sum_n\varrho_{n,n,e,e}^{\mathbf{P}} = -\gamma_1\rho_{e,e}. \quad (A28)$$

For the ground state component we have

$$\dot{\rho}_{g,g} = \sum_n\dot{\varrho}_{n,n,g,g}^{\mathbf{P}} = \gamma_1\sum_{n,p,q}\varrho_{p,q,e,e}^{\mathbf{P}}d_{n,p}d_{n,q}^* = \gamma_1\rho_{e,e},$$
$$\quad (A29)$$

where in the last equality we have used the identity

$$\sum_{n=0}^\infty d_{n,p}d_{n,q}^* = \delta_{pq}. \quad (A30)$$

The off-diagonal terms are the hardest to deal with, but because in the transformed frame, the photon population is initially zero and there is no mechanism to populate $\lambda_{n,m,p,q}$ terms with $\{n,m,p,q\} > 0$ we have

$$\dot{\rho}_{e,g} = \dot{\lambda}_{0,0,0,0} = [-i(\widetilde{\omega}_a + B) - \gamma_1/2 - \gamma_\phi - \Gamma_d]\rho_{e,g}. \quad (A31)$$

The above expressions correspond to the following effective master equation for the qubit:

$$\dot{\rho} = -i\frac{\omega_{ac}}{2}[\sigma_z, \rho] + \gamma_1\mathcal{D}[\sigma_-]\rho + [\gamma_\phi + \Gamma_d]\mathcal{D}[\sigma_z]\rho/2 \equiv \mathcal{L}\rho,$$
$$\quad (A32)$$

where $\omega_{ac} = \widetilde{\omega}_a + B$.

APPENDIX B: DERIVATION OF THE EFFECTIVE QUBIT STOCHASTIC MASTER EQUATION

To derive the effective qubit stochastic master equation we start by using the linear form [39,53,54] of the full SME, Eq. (4.2). This is,

$$\dot{\bar{\varrho}}_J = \mathcal{L}_{\text{tot}}\bar{\varrho}_J + \sqrt{\kappa\eta}\bar{\mathcal{M}}[2I_\phi]\bar{\varrho}_J J + i\sqrt{\kappa\eta}[Q_\phi, \bar{\varrho}_J]J, \quad \text{(B1)}$$

where the bar here is used to signify that the state is not normalized and the linear measurement superoperator is

$$\bar{\mathcal{M}}[c]\varrho = c\varrho/2 + \varrho c/2. \quad \text{(B2)}$$

Moving to the frame defined by Eq. (3.8) gives

$$\dot{\bar{\varrho}}_J^{\mathbf{P}} = \mathcal{L}_{\text{tot}}\bar{\varrho}_J^{\mathbf{P}} + \sqrt{\kappa\eta}[|\beta|\cos(\theta_\beta - \phi)\bar{\mathcal{M}}[\sigma_z]\bar{\varrho}_J^{\mathbf{P}}$$
$$+ |\mu|\cos(\theta_\mu - \phi)\bar{\varrho}_J^{\mathbf{P}} + ae^{-i\phi}\bar{\varrho}_J^{\mathbf{P}} + \bar{\varrho}_J^{\mathbf{P}}a^\dagger e^{i\phi}]J$$
$$\times i\frac{\sqrt{\kappa\eta}|\beta|\sin(\theta_\beta - \phi)}{2}[\sigma_z, \bar{\varrho}^{\mathbf{P}}]J. \quad \text{(B3)}$$

In the same way as Eqs. (A22)–(A25) were obtained, we can write equations of motion for the coefficients $\bar{\varrho}_{n,m,e,e}^{\mathbf{P}}$, $\bar{\varrho}_{n,m,g,g}^{\mathbf{P}}$, and $\bar{\lambda}_{n,m,p,q}$ of the decomposition of the conditional density matrix $\bar{\varrho}_J^{\mathbf{P}}$ in the energy basis. The first term of Eq. (B3) yields the same terms as in Eqs. (A22)–(A25). As a result, we obtain

$$\dot{\bar{\varrho}}_{n,m,e,e}^{\mathbf{P}} = (\text{A22}) + \sqrt{\kappa\eta}[\sqrt{n+1}e^{-i\phi}\bar{\varrho}_{n+1,m,e,e}^{\mathbf{P}}$$
$$+ \sqrt{m+1}e^{i\phi}\bar{\varrho}_{n,m+1,e,e}^{\mathbf{P}} + |\mu|\cos(\theta_\mu - \phi)\bar{\varrho}_{n,m,e,e}^{\mathbf{P}}$$
$$+ |\beta|\cos(\theta_\beta - \phi)\bar{\varrho}_{n,m,e,e}^{\mathbf{P}}]J, \quad \text{(B4)}$$

$$\dot{\bar{\varrho}}_{n,m,g,g}^{\mathbf{P}} = (\text{A23}) + \sqrt{\kappa\eta}[\sqrt{n+1}e^{-i\phi}\bar{\varrho}_{n+1,m,g,g}^{\mathbf{P}}$$
$$+ \sqrt{m+1}e^{i\phi}\bar{\varrho}_{n,m+1,g,g}^{\mathbf{P}} + |\mu|\cos(\theta_\mu - \phi)\bar{\varrho}_{n,m,g,g}^{\mathbf{P}}$$
$$- |\beta|\cos(\theta_\beta - \phi)\bar{\varrho}_{n,m,g,g}^{\mathbf{P}}]J, \quad \text{(B5)}$$

$$\dot{\bar{\lambda}}_{n,m,p,q} = (\text{A25}) + \sqrt{\kappa\eta}[\sqrt{n+1}e^{-i\phi}\bar{\varrho}_{n+1,m,e,g}^{\mathbf{P}}d_{p,q}e^{-i\,\text{Im}[\alpha_g\alpha_e^*]}$$
$$+ \sqrt{m+1}e^{i\phi}\bar{\varrho}_{n,m+1,e,g}^{\mathbf{P}}d_{p,q}e^{-i\,\text{Im}[\alpha_g\alpha_e^*]}$$
$$+ |\mu|\cos(\theta_\mu - \phi)\bar{\lambda}_{n,m,p,q} + i|\beta|\sin(\theta_\beta - \phi)\bar{\lambda}_{n,m,p,q}]J. \quad \text{(B6)}$$

In the above expressions, the equation numbers refer to the RHS of the corresponding expressions. They are the contribution of the Lindblad term $\mathcal{L}_{\text{tot}}\bar{\varrho}_J^{\mathbf{P}}$.

By noting that these matrix elements are not coupled in the qubit basis, we can use the same arguments that were used to obtain Eq. (A31). Doing this, we find for the stochastic parts

$$\dot{\bar{\rho}}_{e,e} = \dot{\bar{\varrho}}_{0,0,e,e}^{\mathbf{P}} = \sqrt{\kappa\eta}[|\mu|\cos(\theta_\mu - \phi) + |\beta|\cos(\theta_\beta - \phi)]\bar{\rho}_{e,e}J, \quad \text{(B7)}$$

$$\dot{\bar{\rho}}_{e,g} = \dot{\bar{\lambda}}_{0,0,0,0} = \sqrt{\kappa\eta}[|\mu|\cos(\theta_\mu - \phi) + i|\beta|\sin(\theta_\beta - \phi)]\bar{\rho}_{e,g}J. \quad \text{(B8)}$$

For the ground state amplitude we have

$$\dot{\bar{\rho}}_{g,g} = \sum_n \dot{\bar{\varrho}}_{n,n,g,g}^{\mathbf{P}} = \sqrt{\kappa\eta}[|\mu|\cos(\theta_\mu - \phi) - |\beta|\cos(\theta_\beta - \phi)]$$
$$\times \bar{\rho}_{g,g}J + \sqrt{\kappa\eta}[(e^{-i\phi}\bar{\varrho}_{1,l}^{\mathbf{P}} + e^{i\phi}\bar{\varrho}_{1,r}^{\mathbf{P}})]J, \quad \text{(B9)}$$

where we have defined

$$\bar{\varrho}_{1,l}^{\mathbf{P}} = \sum_n \sqrt{n+1}\bar{\varrho}_{n+1,n,g,g}^{\mathbf{P}}, \quad \text{(B10)}$$

$$\bar{\varrho}_{1,r}^{\mathbf{P}} = \sum_n \sqrt{n+1}\bar{\varrho}_{n,n+1,g,g}^{\mathbf{P}}. \quad \text{(B11)}$$

The amplitude $\bar{\varrho}_{1,l}^{\mathbf{P}}$ obeys the equations of motion

$$\dot{\bar{\varrho}}_{1,l}^{\mathbf{P}} = -i(\Delta_r - \chi)\bar{\varrho}_{1,l}^{\mathbf{P}} - \kappa\bar{\varrho}_{1,l}^{\mathbf{P}}/2 + \beta\gamma_1\bar{\rho}_{e,e}^{\mathbf{P}}$$
$$+ \sqrt{\kappa\eta}[|\mu|\cos(\theta_\mu - \phi) - |\beta|\cos(\theta_\beta - \phi)]\bar{\varrho}_{1,l}^{\mathbf{P}}J$$
$$+ \sqrt{\kappa\eta}\left[\sum_n \sqrt{(n+2)(n+1)}\bar{\varrho}_{n+2,n,g,g}^{\mathbf{P}}e^{-i\phi}\right.$$
$$\left. + \sum_n n\bar{\varrho}_{n,n,g,g}^{\mathbf{P}}e^{i\phi}\right]J \quad \text{(B12)}$$

and we find a similar equation for $d_t\bar{\varrho}_{1,r}^{\mathbf{P}}$. From this result, we find that provided that

$$\epsilon \equiv \frac{2\gamma_1}{\kappa} \ll 1, \quad \text{(B13)}$$

the effect of $\bar{\varrho}_{1,l}^{\mathbf{P}}$ and $\bar{\varrho}_{1,r}^{\mathbf{P}}$ on $\bar{\rho}_{g,g}^{\mathbf{P}}$ will be very small. In this situation, it is possible to construct a laboratory frame linear SME for the qubit only,

$$\dot{\bar{\rho}}_J = \mathcal{L}\bar{\rho}_J + \sqrt{\kappa\eta}|\beta|\cos(\theta_\beta - \phi)\bar{\mathcal{M}}[\sigma_z]\bar{\rho}_J J$$
$$+ i\frac{\sqrt{\kappa\eta}|\beta|\sin(\theta_\beta - \phi)}{2}[\sigma_z, \bar{\rho}_J]J + \sqrt{\kappa\eta}|\mu|\cos(\theta_\mu - \phi)\bar{\rho}_J J. \quad \text{(B14)}$$

Using Eq. (4.12) and normalizing the above SME gives Eq. (4.8) with measurement record statistics given by Eq. (4.11).

APPENDIX C: INCLUDING COHERENT CONTROL OF THE QUBIT

A drive on the input port of the resonator at a frequency ω_c close to the qubit transition frequency can be used to coherently control the state of the qubit. As shown in Refs. [5,30], this can be represented by the term

$$\frac{\Omega_R}{2}(\sigma_- e^{+i\omega_c t} + \sigma_+ e^{-i\omega_c t}), \quad \text{(C1)}$$

in the qubit-resonator Hamiltonian, Eq. (2.2). In this expression, Ω_R is the Rabi amplitude which depends on the drive amplitude and its detuning to the resonator frequency.

To see how this changes the effective qubit master equations obtained in the previous appendixes, we apply the transformation of Eq. (3.8). In a frame rotating at the frequency ω_c, we find

$$\frac{\Omega_R}{2}(e^{-i\,\text{Im}\{\alpha_g\alpha_e^*\}}\sigma_- D(\beta) + \text{H.c.}). \tag{C2}$$

In this transformed frame, it is apparent that when the qubit flips, it must "drag" the photon field populating the resonator. In this situation, the equation of motion for the coefficients of Eq. (A3) are modified in the following way:

$$\dot{\varrho}_{n,m,e,e}^{\mathbf{P}} = (A22) + i\frac{\Omega_R}{2}\sum_p [\lambda_{n,p,p,m} - \lambda_{m,p,p,n}^*], \tag{C3}$$

$$\dot{\varrho}_{n,m,g,g}^{\mathbf{P}} = (A23) - i\frac{\Omega_R}{2}\sum_p [\lambda_{p,n,m,p} - \lambda_{p,n,m,p}^*], \tag{C4}$$

$$\dot{\lambda}_{n,m,p,q} = (A25) - i\frac{\Omega_R}{2}\sum_l [\varrho_{l,m,g,g}^{\mathbf{P}}d_{l,n}^* - \varrho_{n,l,e,e}^{\mathbf{P}}d_{m,l}^*]d_{p,q}, \tag{C5}$$

where the equation numbers refer to the RHS of the corresponding expressions. These additional terms mix the various coefficients of the decomposition of ρ and obtaining an effective master equation for the qubit only is no longer possible exactly. This can nevertheless be done in the small measurement amplitude limit.

The case where a control and a measurement drive are acting on the system simultaneously is most interesting in the case where the measurement drive is of small amplitude. For example, in Ref. [7], a weak continuous measurement drive corresponding to about one photon was used to monitor Rabi oscillations. When the measurement drive amplitude is increased, the qubit is dephased faster and coherent control is realized with less fidelity.

In the weak measurement limit $\beta \to 0$, the matrix element of the displacement operator $d_{n,m}$ in the photon number basis can be approximated to

$$d_{p,q} = e^{-|\beta|^2/2}\sqrt{\frac{\min(p,q)!}{\max(p,q)!}}$$

$$\times L_{\min(p,q)}^{\text{abs}(p-q)}(|\beta|^2)\begin{cases} \beta^{p-q}, & p > q, \\ (-\beta^*)^{q-p}, & q > p \end{cases}$$

$$\approx e^{-|\beta|^2/2}\sqrt{\frac{\min(p,q)!}{\max(p,q)!}}[1 - (\max(p,q) + 1/2)|\beta|^2]$$

$$\times \begin{cases} \beta^{p-q}, & p > q, \\ (-\beta^*)^{q-p}, & q > p, \end{cases} \tag{C6}$$

where $L_n^m(x)$ is an associated Laguerre polynomial. To lowest order in β, this reduces $d_{p,q} \sim \delta_{p,q}$. Making this replacement in the above expressions for the amplitudes, we find in this limit the following effective qubit master equation:

$$\dot{\rho} = -i\frac{\tilde{\omega}_a + B}{2}[\sigma_z, \rho] - i\frac{\Omega_R}{2}[\sigma_x, \rho] + \gamma_1\mathcal{D}[\sigma_-]\rho$$

$$+ [\gamma_\phi + \Gamma_d]\mathcal{D}[\sigma_z]\rho/2. \tag{C7}$$

Unsurprisingly, in the small β limit, the only effect of a control drive is to flip the qubit at the Rabi frequency Ω_R. If we were to include the next order in $d_{p,q}$ we would not be able to obtain an equation for just the qubit, effects such as sidebands would be observed.

[1] H. J. Carmichael, *An Open Systems Approach to Quantum Optics* (Springer-Verlag, New York, 1993).

[2] C. Gardiner and P. Zoller, *Quantum Noise: A Handbook of Markovian and Non-Markovian Quantum Stochastic Methods with Applications to Quantum Optics* (Springer, New York, 2004).

[3] H. M. Wiseman and L. Diósi, Chem. Phys. **268**, 91 (2001).

[4] K. Mølmer, Y. Castin, and J. Dalibard, J. Opt. Soc. Am. B **10**, 524 (1993).

[5] A. Blais, R. S. Huang, A. Wallraff, S. M. Girvin, and R. J. Schoelkopf, Phys. Rev. A **69**, 062320 (2004).

[6] A. Wallraff, D. I. Schuster, A. Blais, L. Frunzio, R. S. Huang, J. Majer, S. Kumar, S. M. Girvin, and R. J. Schoelkopf, Nature (London) **431**, 162 (2004).

[7] A. Wallraff, D. I. Schuster, A. Blais, L. Frunzio, J. Majer, M. H. Devoret, S. M. Girvin, and R. J. Schoelkopf, Phys. Rev. Lett. **95**, 060501 (2005).

[8] D. I. Schuster, A. Wallraff, A. Blais, L. Frunzio, R. S. Huang, J. Majer, S. M. Girvin, and R. J. Schoelkopf, Phys. Rev. Lett. **94**, 123602 (2005).

[9] J. Gambetta, A. Blais, D. I. Schuster, A. Wallraff, L. Frunzio, J. Majer, M. H. Devoret, S. M. Girvin, and R. J. Schoelkopf, Phys. Rev. A **74**, 042318 (2006).

[10] J. Q. You and F. Nori, Phys. Rev. B **68**, 064509 (2003).

[11] G. D. Mahan, *Many Particle Physics* (Springer, New York, 2000).

[12] H. M. Wiseman and G. J. Milburn, Phys. Rev. A **47**, 642 (1993).

[13] A. N. Korotkov, Phys. Rev. B **60**, 5737 (1999).

[14] A. N. Korotkov, Phys. Rev. B **63**, 115403 (2001).

[15] A. N. Korotkov and D. V. Averin, Phys. Rev. B **64**, 165310 (2001).

[16] H. M. Wiseman, D. Wahyu Utami, H. B. Sun, G. J. Milburn, B. E. Kane, A. Dzurak, and R. G. Clark, Phys. Rev. B **63**, 235308 (2001).

[17] H.-S. Goan, G. J. Milburn, H. M. Wiseman, and H. B. Sun, Phys. Rev. B **63**, 125326 (2001).

[18] A. N. Korotkov, Phys. Rev. B **67**, 235408 (2003).

[19] N. P. Oxtoby, P. Warszawski, H. M. Wiseman, H.-B. Sun, and R. E. S. Polkinghorne, Phys. Rev. B **71**, 165317 (2005).

[20] N. P. Oxtoby, J. Gambetta, and H. M. Wiseman, e-print arXiv:0706.3527.

[21] A. C. Doherty and K. Jacobs, Phys. Rev. A **60**, 2700 (1999).

[22] M. I. Dykman and M. A. Krivoglaz, Sov. Phys. Solid State **29**,

210 (1987).

[23] D. I. Schuster, A. A. Houck, J. A. Schreier, A. Wallraff, J. M. Gambetta, A. Blais, L. Frunzio, J. Majer, B. Johnson, M. H. Devoret, S. M. Girvin, and R. J. Schoelkopf, Nature (London) **445**, 515 (2007).

[24] H.-P. Breuer and F. Petruccione, *The Theory of Open Quantum Systems* (Oxford University Press, Oxford, 2002).

[25] M. J. Gagen and G. J. Milburn, Phys. Rev. A **47**, 1467 (1993).

[26] C. Presilla, R. Onofrio, and U. Tambini, Ann. Phys. (N.Y.) **248**, 95 (1996).

[27] J. D. Cresser, S. M. Barnett, J. Jeffers, and D. T. Pegg, Opt. Commun. **264**, 352 (2006).

[28] A. A. Houck, D. I. Schuster, J. M. Gambetta, J. A. Schreier, B. R. Johnson, J. M. Chow, J. Majer, L. Frunzio, M. H. Devoret, S. M. Girvin, and R. J. Schoelkopf, Nature (London) **449**, 328 (2007).

[29] J. Majer, J. M. Chow, J. M. Gambetta, J. Koch, B. R. Johnson, J. A. Schreier, L. Frunzio, D. I. Schuster, A. A. Houck, A. Wallraff, A. Blais, M. H. Devoret, S. M. Girvin, and R. J. Schoelkopf, Nature (London) **449**, 443 (2007).

[30] A. Blais, J. Gambetta, A. Wallraff, D. I. Schuster, S. M. Girvin, M. H. Devoret, and R. J. Schoelkopf, Phys. Rev. A **75**, 032329 (2007).

[31] J. Koch, T. M. Yu, J. Gambetta, A. A. Houck, D. I. Schuster, J. Majer, A. Blais, M. H. Devoret, S. M. Girvin, and R. J. Schoelkopf, Phys. Rev. A **76**, 042319 (2007).

[32] M. Boissonneault, J. Gambetta, and A. Blais (unpublished).

[33] G. Lindblad, Commun. Math. Phys. **2**, 119 (1976).

[34] In the dispersive regime, the operators describing damping, dephasing, and measurement should by transformed in the same way as the Hamiltonian. This leads to corrections at order (g/Δ) and can be ignored here. These effects where briefly described in [5] and are investigated in detail in [32].

[35] V. Bonzom, H. Bouzidi, and P. Degiovanni, e-print arXiv:0704.3489.

[36] A. J. Leggett, S. Chakravarty, A. T. Dorsey, M. P. A. Fisher, A. Garg, and W. Zwerger, Rev. Mod. Phys. **59**, 1 (1987).

[37] E. K. Irish, J. Gea-Banacloche, I. Martin, and K. C. Schwab, Phys. Rev. B **72**, 195410 (2005).

[38] M. A. Nielsen and I. L. Chuang, *Quantum Computation and Quantum Information* (Cambridge University Press, Cambridge, UK, 2000).

[39] J. Gambetta and H. M. Wiseman, J. Opt. B: Quantum Semiclassical Opt. **7**, S250 (2005).

[40] In Ref. [12] only Lindblad superoperators with one decoherence term are considered and as such a pure state unraveling is possible, here however we have three decoherence terms and only unravel one of them. That is, we have a partial measurement and must use a SMEs unless we use the numerical techniques of Ref. [39].

[41] C. W. Gardiner, *Handbook of Stochastic Methods: For Physics, Chemistry and the Natural Science* (Springer-Verlag, Berlin, 1985).

[42] H. M. Wiseman and G. J. Milburn, Phys. Rev. A **47**, 1652 (1993).

[43] J. Gambetta, W. A. Braff, A. Wallraff, S. M. Girvin, and R. J. Schoelkopf, Phys. Rev. A **76**, 012325 (2007).

[44] M. H. Devoret and R. J. Schoelkopf, Nature (London) **406**, 1039 (2000).

[45] D. Averin, in *Exploring the Quantum Classical Frontier: Recent Advances in Macroscopic Quantum Phenomena*, edited by J. R. Friedman and S. Han (Nova Science, 2002), Chap. 14, pp. 447–470.

[46] A. A. Clerk, S. M. Girvin, and A. D. Stone, Phys. Rev. B **67**, 165324 (2003).

[47] Y. Makhlin, G. Schön, and A. Shnirman, Rev. Mod. Phys. **73**, 357 (2001).

[48] N. P. Oxtoby, H. M. Wiseman, and H.-B. Sun, Phys. Rev. B **74**, 045328 (2006).

[49] J. Gambetta, A. Blais, C. Cheung, R. Schoelkopf, and S. M. Girvin (unpublished).

[50] D. Walls and G. Milburn, *Quantum Optics* (Springer-Verlag, Berlin, 1994).

[51] A. Imamoglu, Phys. Rev. A **50**, 3650 (1994).

[52] J. Gambetta and H. M. Wiseman, Phys. Rev. A **66**, 052105 (2002).

[53] H. M. Wiseman, Quantum Semiclassic. Opt. **8**, 205 (1996).

[54] P. Goetsch and R. Graham, Phys. Rev. A **50**, 5242 (1994).